Electronic Supplementary Material (ESI) for Journal of Materials Chemistry C.

Supplemental information

Spin-polarization anisotropy controlled by bending in tungsten diselenide nanoribbons and tunable excitonic states

Hong Tang, Santosh Neupane, Li Yin, Jason M. Breslin, and Adrienn Ruzsinszky

Department of Physics, Temple University, Philadelphia, PA 19122

The contents and organization in the Supplemental Information

Note 1. Spin polarization anisotropy analyses for A12WSe2 and A7WSe2 nanoribbons

The $A12WSe_2$ nanoribbon also shows a similar spin polarization anisotropy with bending, as presented in SI Figures S19-S21. The spin polarization in the x direction also generally increases with increasing bending curvatures, while in the y direction, it generally decreases with bending, and in the periodic z direction, it generally remains small. From flat to $R = 13$ Å, the spin polarization along the x axis shows a symmetric feature among energy degenerate odd and even indexed bands and electron and hole doping will not result in a net magnetization in the x direction. $R = 12$ Å is the first critical bending radius R_1. For $R = 12$ Å, $R = 11$ Å, and $R = 10$ Å, the band gaps become indirect, and the bottom of the upper edge bands is spin-down dominant, while the top of the lower edge bands does not show an obvious specific spin dominancy. This means that an electron doping results in a net magnetization point to the positive x direction, while hole doping results in no net magnetization along the x axis. At $R = 9$ Å or $R = 8$ Å, the second critical bending radius R_2 for $A12WSe_2$, the bottom of the upper edge bands becomes spin-up dominant, opposite to the cases of $R = 12$ Å, $R = 11$ Å, and $R = 10$ Å, although the top of the valence bands still does not show an obvious dominancy. It means that an electron doped $A12WSe_2$ will flip the direction of the net magnetization along the x axis when crossing R_2. At $R = 8$ Å the lower edge bands merge into VBC. For larger bending ($R = 7$Å and $R = 6$ Å), the bottom of the upper edge bands is spin-up dominant, while the top of the valence bands shows an obvious spin-down dominancy. The different altering trend of the spin polarization anisotropy in the $A12WSe_2$ nanoribbon in comparison with $A13WSe_2$ may be due to the slightly short width of the $A12WSe_2$ ribbon and its asymmetric edge structures.

For the narrow $A7WSe_2$ nanoribbon, the x-direction spin polarization shows a symmetric feature among the odd and even indexed bands for flat, $R = 16$ Å, $R = 10$ Å and $R = 7$ Å, where the electron and hole doping will not result in a net magnetization in the x direction, see SI Figures S26-S28. At $R = 5$ Å, the four bands just below the Fermi level (two for odd indexed and another two for even indexed bands) show an asymmetric spin-polarization feature, while the upper edge bands still show a symmetric one. The top of the valence bands is slightly spin-down dominated, which means a hole doping will result in a net magnetization towards the negative x direction. The spin polarizations of the bands along the y direction show a symmetric feature between the odd and even indexed bands for all bending cases, while along the z direction, the spin-polarization is almost negligibly small. The electron and hole doping will not result in a net magnetization in the y and z directions.

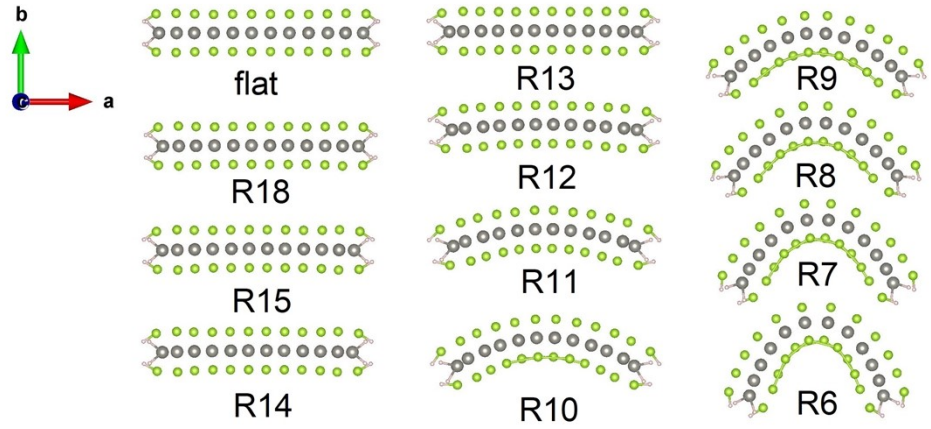

Figure S1. The relaxed structures of the A12WSe2 nanoribbon. R18 represents the bending radius $R = 18\text{Å}$, and so on for others.

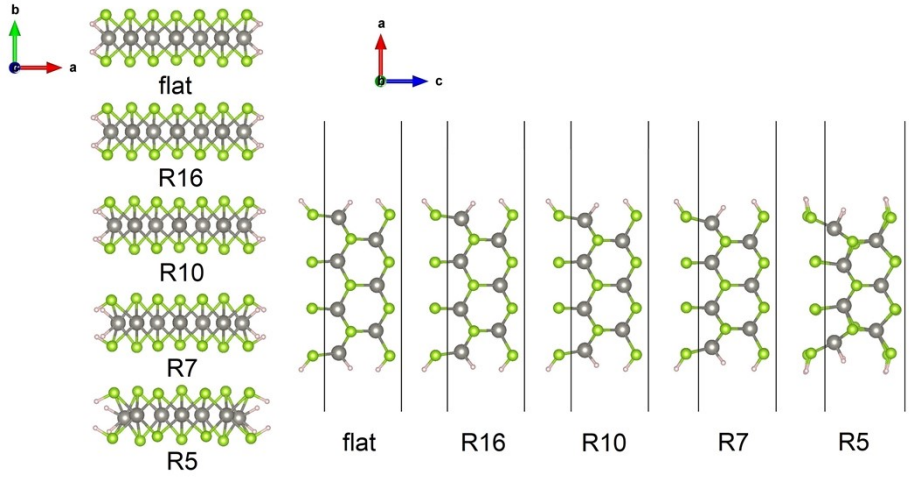

Figure S2. The relaxed structures of the A7WSe2 nanoribbon.

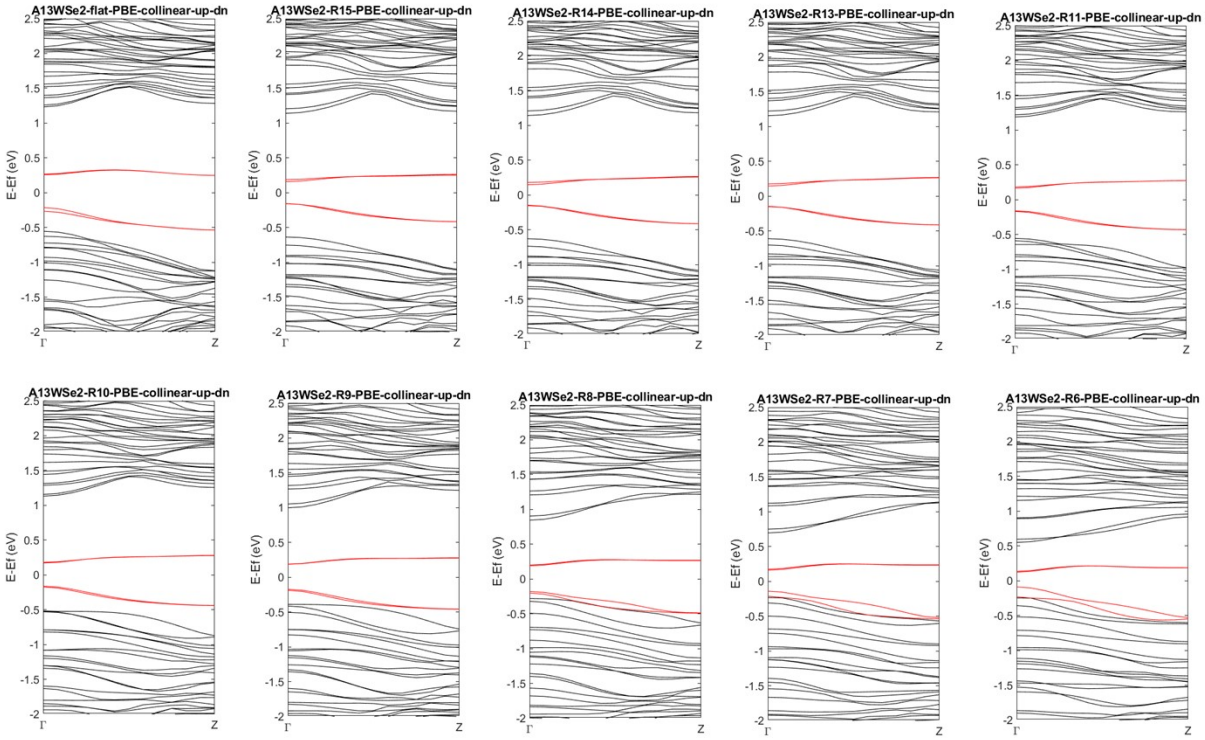

Figure S3. The band structures of A13WSe2 nanoribbon under different bending radii calculated with PBE and without the SOC effect included. See the title on each plot for the bending radius.

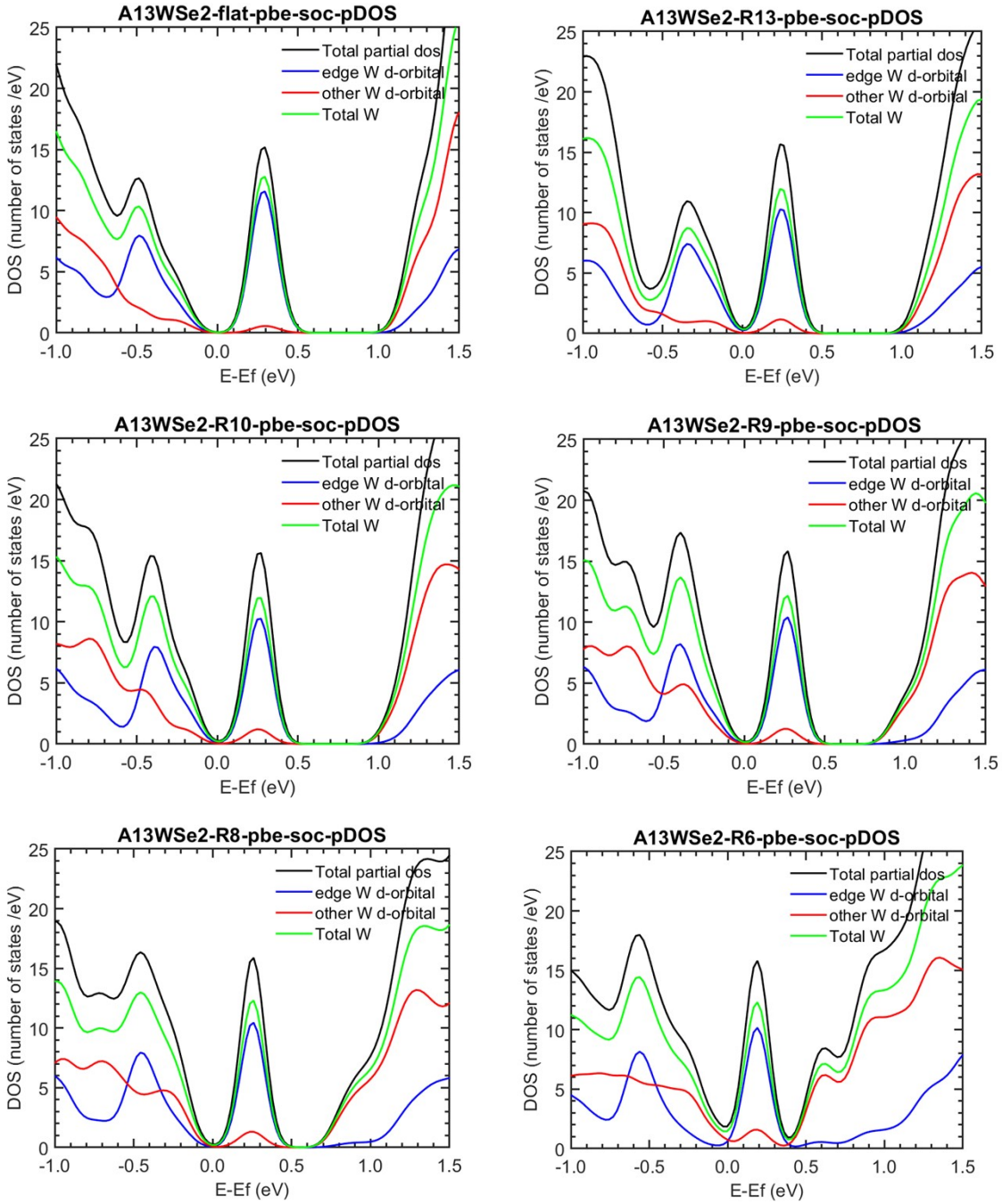

Figure S4. The analysis of the density of states of A13WSe2 nanoribbon under different bending radii calculated with PBE and the SOC effect included. See the title on each plot for the bending radius.

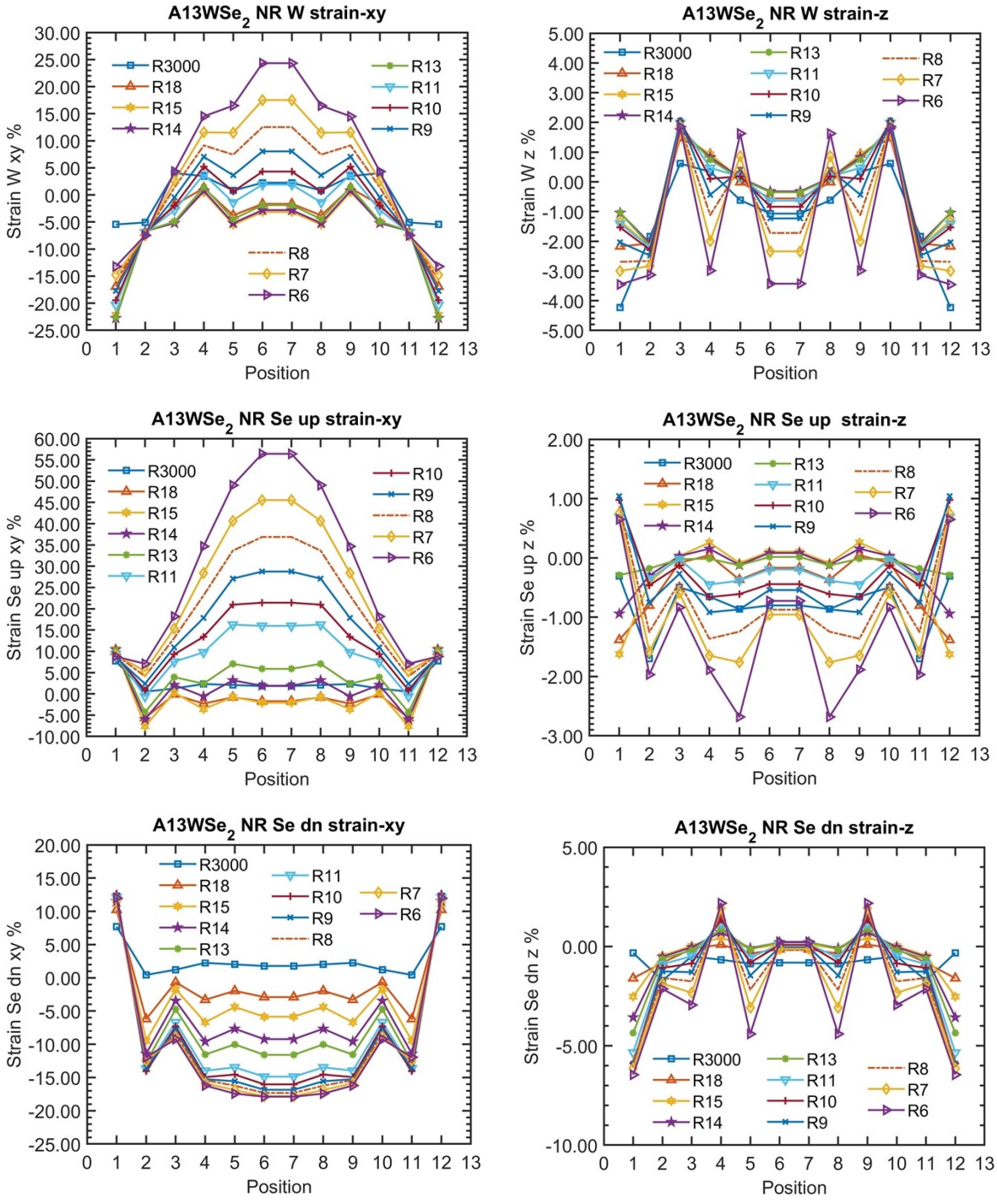

Figure S5. The strains in the A13WSe2 nanoribbon under different bending radii calculated with PBE and the SOC effect included. See the title on each plot for the type of strains, where strain-xy means the strainin the xy plane, and strain-z for strain in the z direction. Detailed definitions see Ref. 23 in the main text.

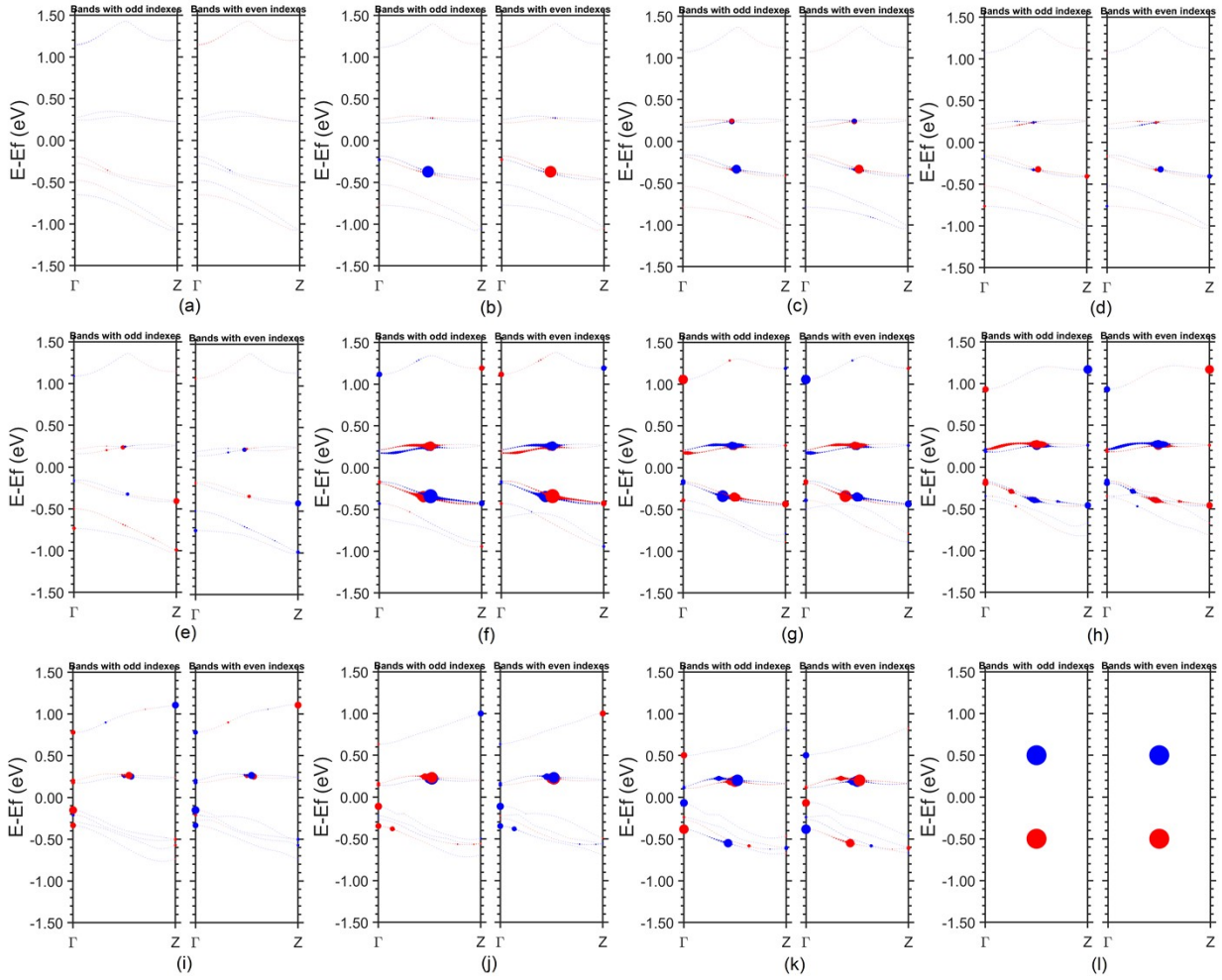

Figure S6. The k point and band resolved spin polarization along the z axis (along the periodical direction of the nanoribbon) of the A13WSe_2 nanoribbon under different bending curvature radii R calculated with PBE+SOC. Panels (a), (b), (c), (d), (e), (f), (g), (h), (i), (j), (k), and (l) are for flat, $R = 18$ Å, $R = 15$ Å, $R = 14$ Å, $R = 13$ Å, $R = 11$ Å, $R = 10$ Å, $R = 9$ Å, $R = 8$ Å, $R = 7$ Å, and $R = 6$ Å, respectively. In each panel, the left subplot is for odd number indexed bands, while the right one is for the even number indexed bands. The red (blue) color represents the spin-up (spin-down) spin polarization, with the spin-up (spin-down) points to the negative (positive) direction of the z axis. The magnitude of the magnetic moment (in the unit of Bohr magneton μ_B) at each k point and each band is proportional to the size of the spot. Panel (l) represents the reference size of the spots with the magnetic moment of 1 μ_B (red) or -1 μ_B (blue).

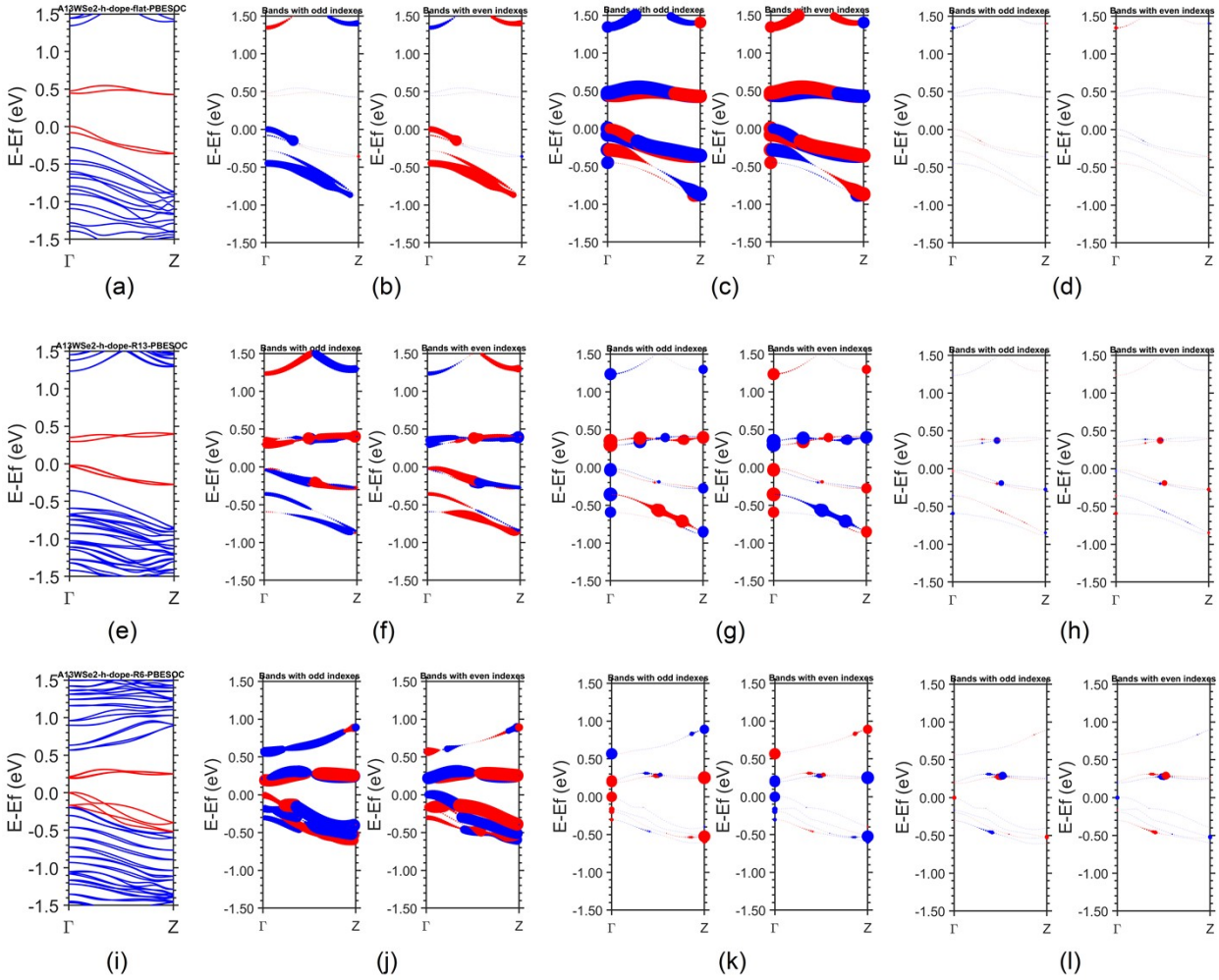

Figure S7. The band structures and k point and band resolved spin polarizations of the A13WSe2 nanoribbon under the hole doping of 0.12 holes per supercell and under three bending conditions calculated with PBE+SOC. Panels (a), (b), (c), and (d) in the top row are the band structure, spin polarization along the x axis, spin polarization the y axis, and spin polarization along the z axis, respectively, for the flat nanoribbon. In panels (b)-(d), the odd number indexed bands are plotted on the left side and the even numbered ones are on the right side with the same energy scale, for clarity. The middle (bottom) row is for bending radius $R = 13$ Å ($R = 6$ Å). The figure panels in the last two rows are arranged similarly as in the top row.

Note 2. The d-orbital decomposition analyses for A13WSe2.

Since the W d-orbital makes the significantly large contribution to the density of states around the Fermi level, we analyzed the d-orbital decomposed spin-polarization in the band structures of the A13WSe2 nanoribbon under different bending curvatures. In this section of discussion, the spin-polarization is referred to the one decomposed on the five d-orbitals (d_{z^2}, $d_{x^2-y^2}$, d_{xy}, d_{yz}, d_{xz}).

For better understanding, we first make some definitions. For the A13WSe2 nanoribbon, the structure of the nanoribbon is mirror symmetric about the plane parallel with the yz plane and passing W4 (the middle W atom with atom index 4), as shown in Figure S8 for the structure and atom indexes. The W atoms 1 and 7 locate at symmetric positions and form a pair P1-7, similarly for atom pairs P2-6, P3-5, P8-13, P9-12, and P10-11. Atom W4 is single. In a band structure, the band indexes are denoted as $2n-1$ and $2n$ for an odd number indexed band and an even number indexed band, respectively, where $n = 1, 2, 3,\ldots$. Accordingly, a state in the band structure is denoted as $S_{2n-1,k}$ or $S_{2n,k}$, where k is the crystal momentum or k point, and $2n-1$ and $2n$ are for an odd number band index and an even number band index, respectively. For a band state $S_{2n-1,k}$ (or $S_{2n,k}$), each W atom will produce five decomposed spin-polarizations along each of the three spatial axes x, y, and z, corresponding to the five d-orbitals (d_{z^2}, $d_{x^2-y^2}$, d_{xy}, d_{yz}, d_{xz}), resulting in totally 15 decompositions for each W atom. Figures S9 to S14 show the plots of the band structure map of the d-orbital decomposed spin-polarization along the x and y axis for each W atom in the A13WSe2 nanoribbon under three different bending conditions. In all cases, the spin-polarization decomposed in the z axis direction is negligibly small and not shown in the Figures. By inspecting the plots, we have five observations (Y1 to Y5). Their applicability for cases of different bending and spatial directions is listed in Table S1.

For the flat nanoribbon, the odd number ($2n-1$) indexed band (OB) is always associated with the even number ($2n$) indexed band (EB) and they form a paired OB and EB (POBEB). The OB and EB in a POBEB are almost degenerate in energy. For the spin-polarization along the y axis, the applicability of the five observations is the following. (Y1.) for a given W atom, the state $S_{2n-1,k}$ in OB and the state $S_{2n,k}$ in EB in a POBEB have the opposite directions of the spin polarization for a given d-orbital decomposition. (Y2.) for a give d-orbital, the W atoms 1 and 7 in pair P1-7 contribute to the magnitude of the spin-polarization in the OB and EB in a POBEB strongly unevenly, i.e., atom 1 contributes much more to EB and much less to OB, while atom 7 does oppositely. (Y3.) for a given d-orbital, atoms 1 and 7 in pair P1-7 produce the same spin direction (up or down) for a given state in the band structure. (Y4.) for either atom in pair P1-7, the directions (up or down) of the spin-polarization decomposed from the different d-orbitals are the same for a given state in the band structure. (Y5.) for a given d orbital, the W atoms near the same edge of the nanoribbon, such as atoms 1 and 8 (or atoms 7 and 13) produce the same spin direction for a given band state. Together Y3-Y5, it shows that all the W atoms with all the five d-orbital decomposition produce the same spin direction of the spin-polarization for a given band state, although with different magnitudes. This results in a totally strong spin-polarization along the y axis in the bands for the flat nanoribbon. Other W atom pairs, such as P2-6, P3-5, P8-13, P9-12, and P10-11, behave similarly in observations Y2 to Y5, while the atom pairs in the middle region of the nanoribbon contribute marginally to the spin-polarization. The W atom pairs near the edge, such as P1-7 and P8-13, produce a strong magnitude of the spin-polarization in the relevant band states and they dominate the contribution to the spin-polarization. The single atom W4 has a negligible contribution to the spin-polarization along the y axis. For a monolayer WSe2, the valence band top has a character of d_{z^2}, and the other four non-bonding $d_{x^2-y^2}$, d_{xy}, d_{yz}, and d_{xz} remain unoccupied [1]. For the flat A13WSe2

nanoribbon, both the lower and upper edge bands have d_{z^2}, $d_{x^2-y^2}$, and d_{xz} characters, due to the formation of edges and the coupling (or interaction) between edges.

For bent nanoribbons at $R = 13$ Å and $R = 6$ Å, for the decomposition along the y axis, the striking difference is in the observation Y3, compared to the flat case. It is that atoms 1 and 7 in pair P1-7 produce the opposite spin direction for a given band state in the band structure, and so do other pairs. This leads to a totally small spin-polarization along the y axis for the bent ribbons. For R13, beside the d_{z^2}, $d_{x^2-y^2}$, and d_{xz} characters, the lower and upper edge bands have additional d_{xy} character. For R6, beside d_{z^2}, $d_{x^2-y^2}$, and d_{xy} characters, the d_{yz} character appears in the lower and upper edge bands, while the d_{xz} character is reduced. This may relate to the tilting of the 2H phase trigonal prism located near the ribbon edges with bending. The tilting angle with respect to the y axis is much larger in R6 than in R13. In R6, the W4 atom, located at the center of the ribbon, is special. It contributes majority of the spin-polarization of the top of the valence bands along the x axis. The trigonal prism centered at W4 is highly strained in R6, where the two top Se atoms are stretched along the x axis, while the two lower Se atoms are compressed. We separated the trigonal prism centered at W4 and treated it as a 7-atom complex and calculated its spin-polarization (results not shown here). It indeed shows that its spin-polarization is aligned along the x direction, while in the y axis direction, the spin-polarization is almost negligible.

It is interesting that the observation Y4, which states that for a given atom, the directions (up or down) of the spin-polarization decomposed from the different d-orbitals are the same for a given band state, is obeyed by almost all the W atoms, except the center W4 atom in R6, further highlights the specialty of this W atom. The observation Y5, which states that the W atoms located on the same edge side of the nanoribbon produce the spin-polarization additively in the band states, is unanimously obeyed by all cases, underscoring the mirror symmetry of the nanoribbon about the center plane passing W4. The observation Y2, which states that the two atoms from the two-edge pair produce an asymmetric distribution in the magnitude of the decomposed spin-polarization in the odd number indexed and even number indexed bands, is also very interesting, and it is only obeyed by the d-orbital decomposition of the spin-polarization along the y axis of the flat and R18 nanoribbons. This may indicate an underlying relation between the additional mirror symmetry about the central W layer of the flat nanoribbon and the y-axis-direction decomposition, since the relaxed structure of R18 is also almost flat, similar with the flat nanoribbon.

1. Manish Chhowalla, Hyeon Suk Shin, Goki Eda, Lain-Jong Li, Kian Ping Loh and Hua Zhang, The chemistry of two-dimensional layered transition metal dichalcogenide nanosheets, Nat. Chem., 2013, 5, 263.

Table S1. The applicability of the five observations (Y1 to Y5) to the band structure map of the d-orbital decomposition of the spin-polarization along the x and y axes for the A13WSe2 nanoribbon under different bending conditions. The key words of the applicability, such as opposite, same, uneven, etc. are underlined in the description in the first column.

Observations	Flat, R18		R13		R6	
	Axis y	Axis x	Axis y	Axis x	Axis y	Axis x
(Y1.) for a given W atom, the state $S_{2n-1,k}$ in OB and the state $S_{2n,k}$ in EB in a POBEB have the <u>opposite directions</u> of the spin polarization for a given d-orbital.	Yes (opposite direction)	Yes (opposite direction)	No (same direction)	Not strict (may opposite or same)	No (same direction, for upper edge bands), Not applicable for bands near VBM*	No (same direction, for upper edge bands), Not applicable for bands near VBM*
(Y2.) for a give d-orbital, the W atoms 1 and 7 in pair P1-7 contribute to the magnitude of the spin-polarization in the OB and EB in a POBEB strongly <u>unevenly</u>, i.e., atom 1 contributes much more to EB and much less to OB, while atom 7 does oppositely.	Yes (unevenly)	No (almost evenly)	No (almost evenly)	No (almost evenly)	No (almost evenly)	No (almost evenly)
(Y3.) for a given d-orbital, atoms 1 and 7 in pair P1-7 produce the <u>same spin direction</u> (up or down) for a given state in the band structure. So do other pairs.	Yes (same direction)	Yes (same direction)	No (opposite direction)	Yes (same direction)	No (opposite direction)	Yes (same direction)
(Y4.) for a given atom, the directions (up or down) of the spin-polarization decomposed from the different d-orbitals are the <u>same</u> for a given state in the band structure.	Yes (same)	Yes (same)	Yes (same)	Yes (for bands near Fermi level)	Yes (same)	Yes (except atom W4)
(Y5.) for a given d orbital, the W atoms near the same edge of the nanoribbon, such as atoms 1 and 8 (or atoms 7 and 13) produce the <u>same spin direction</u> for a given band state.	Yes (same spin direction)	Yes (same spin direction)	Yes (same spin direction)	Yes (same spin direction)	Yes (same spin direction)	Yes (same spin direction)

* At bending radius $R = 6$ Å, the lower edge bands are merged into the valence band continuum. The bands around the valence band maximum (VBM) have a strong splitting. The concept POBEB (the paired odd number indexed band and even number indexed band) may not be well appliable.

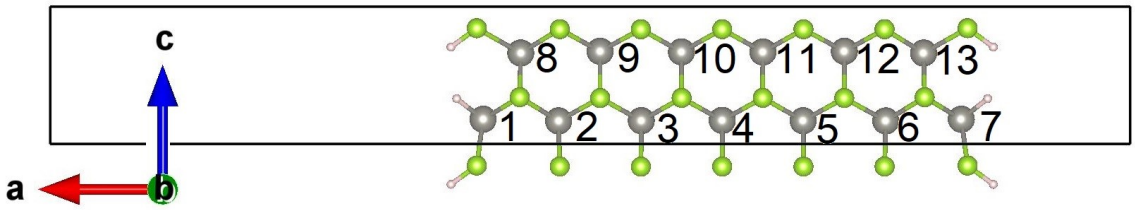

Figure S8. The structure of the A13WSe2 nanoribbon and the atom indexes for the W atoms in the supercell.

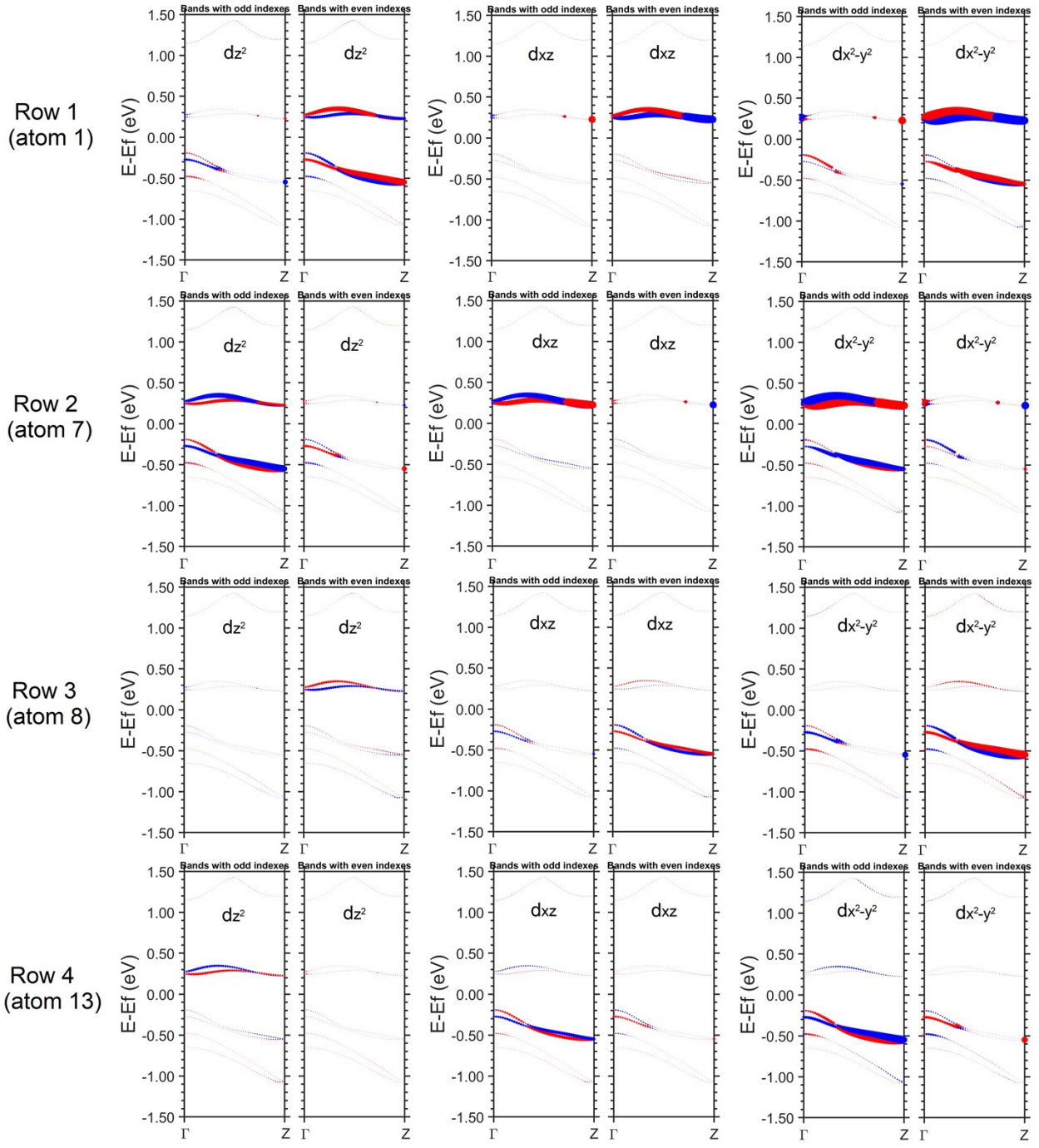

Figure S9. The band structure maps of the d-orbital-decomposed spin-polarization along the y axis for the W atoms in the flat A13WSe2 nanoribbon. Each row is for a specific W atom marked by the atom index. Each panel is for a specific d-orbital decomposition. For example, the panel marked with d_{z^2} is for the decomposed spin-polarization on the d_{z^2} orbital of that corresponding atom. In each d-orbital panel, the left subplot is for the odd number indexed bands and the right one is for the even number indexed bands. The atoms and the d-orbital panels only with significant contribution are shown.

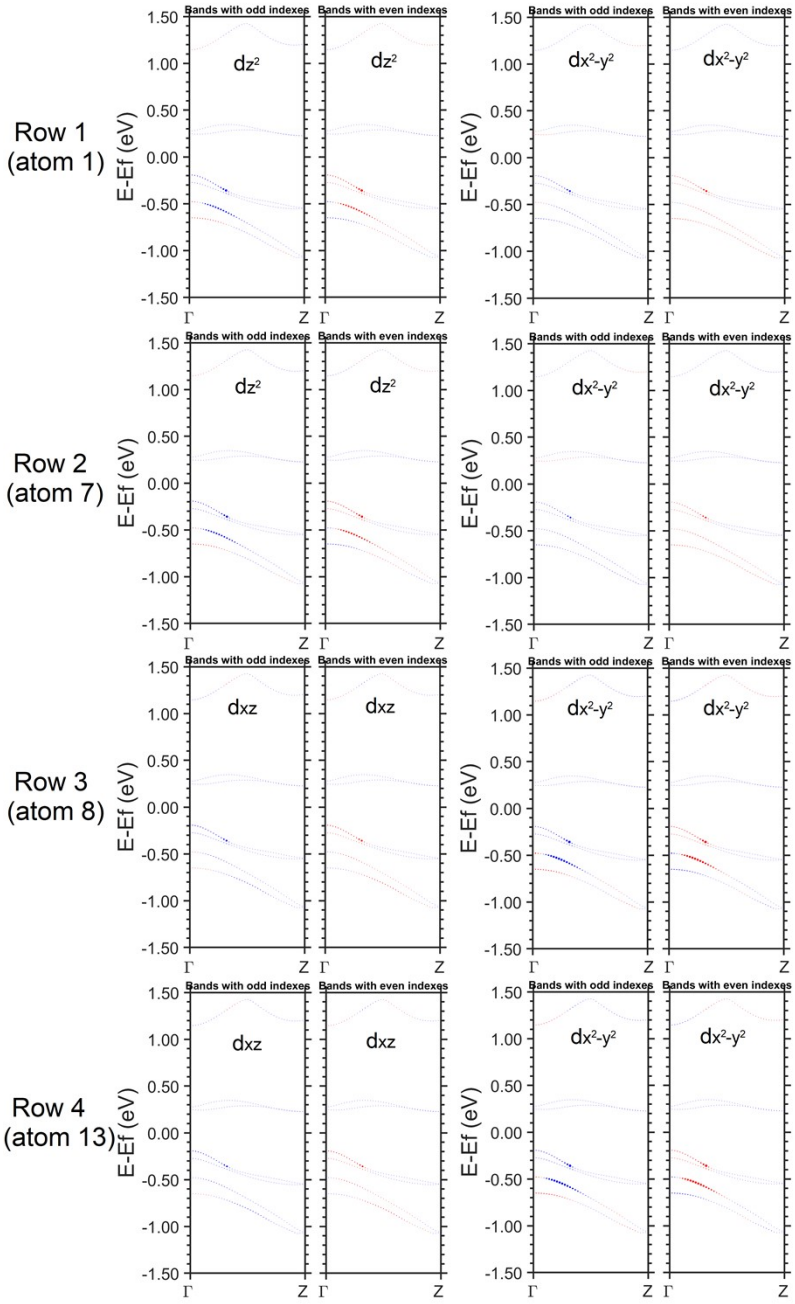

Figure S10. The band structure maps of the d-orbital-decomposed spin-polarization along the x axis for the W atoms in the flat A13WSe2 nanoribbon. Plots are organized in the same way as in Figure S9.

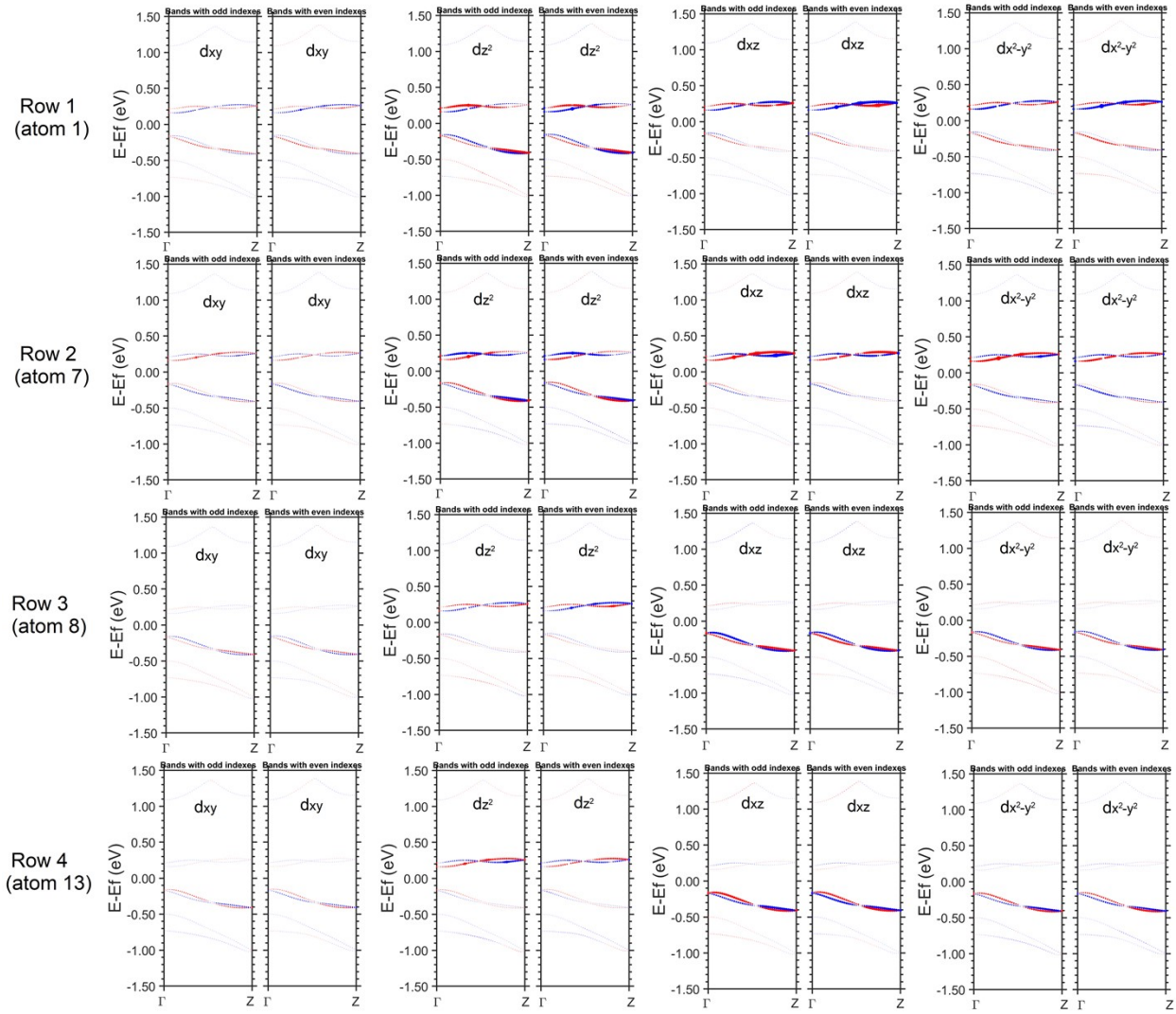

This figure is continued to the next page.

Continued figure to the previous page.

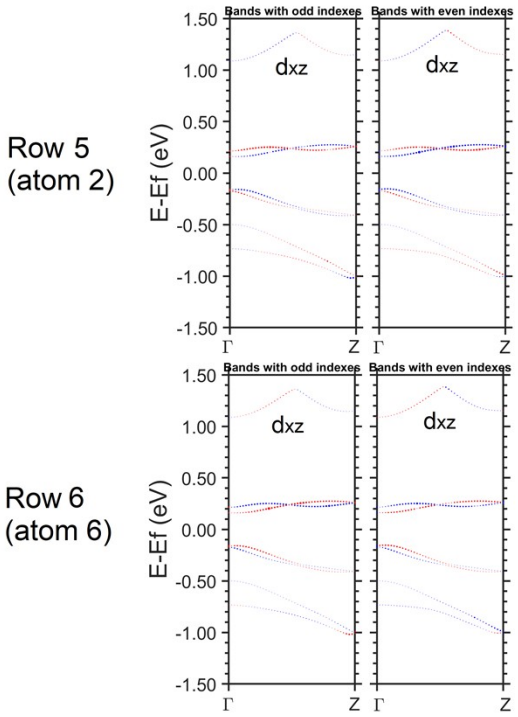

Figure S11. The band structure maps of the d-orbital-decomposed spin-polarization along the y axis for the W atoms in the A13WSe2 nanoribbon under bending curvature radius $R = 13$ Å. The full figure is split, also see the previous page. Plots are organized in the same way as in Figure S9.

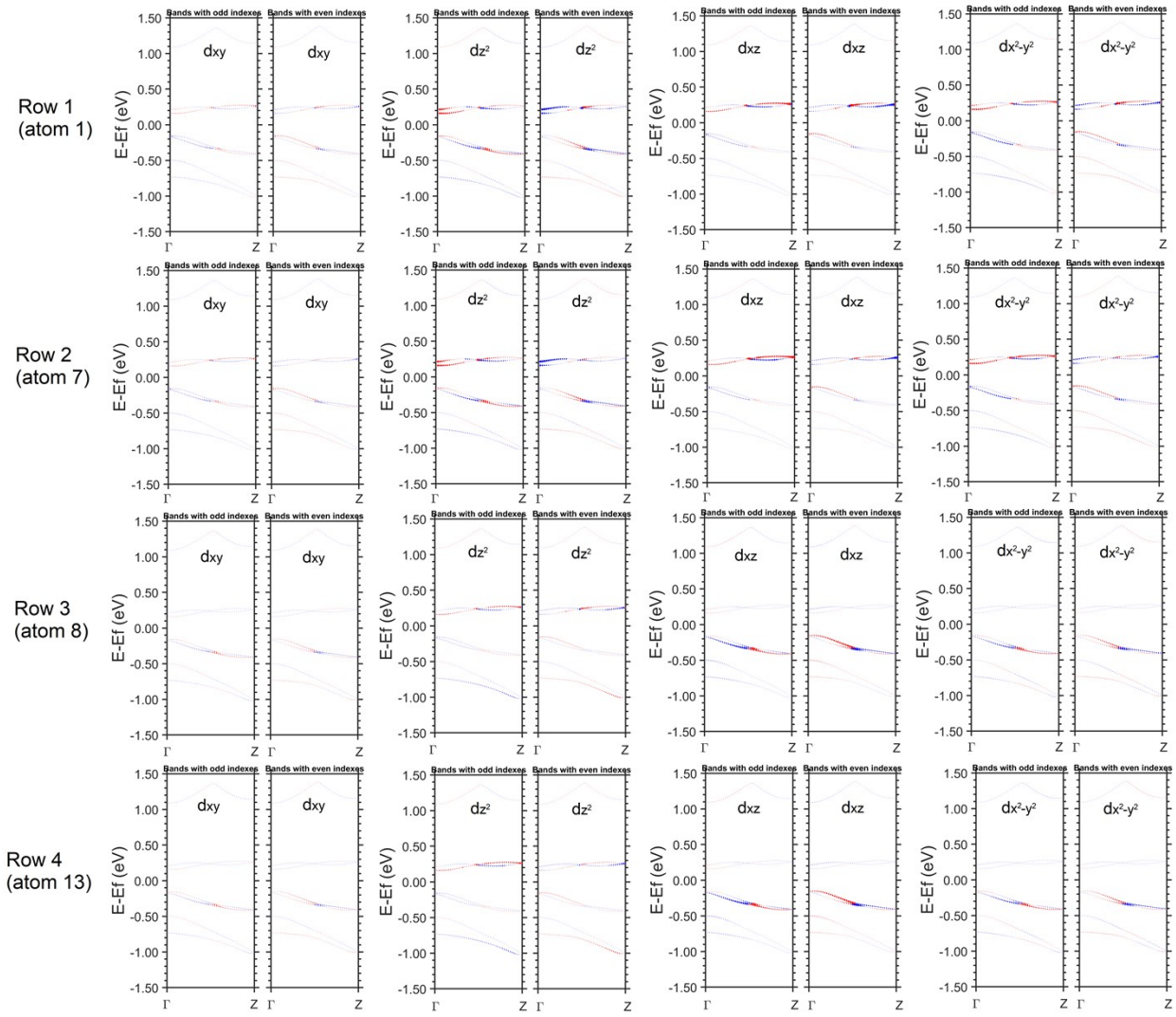

Figure S12. The band structure maps of the d-orbital-decomposed spin-polarization along the x axis for the W atoms in the A13WSe2 nanoribbon under bending curvature radius $R = 13$ Å. Plots are organized in the same way as in Figure S9.

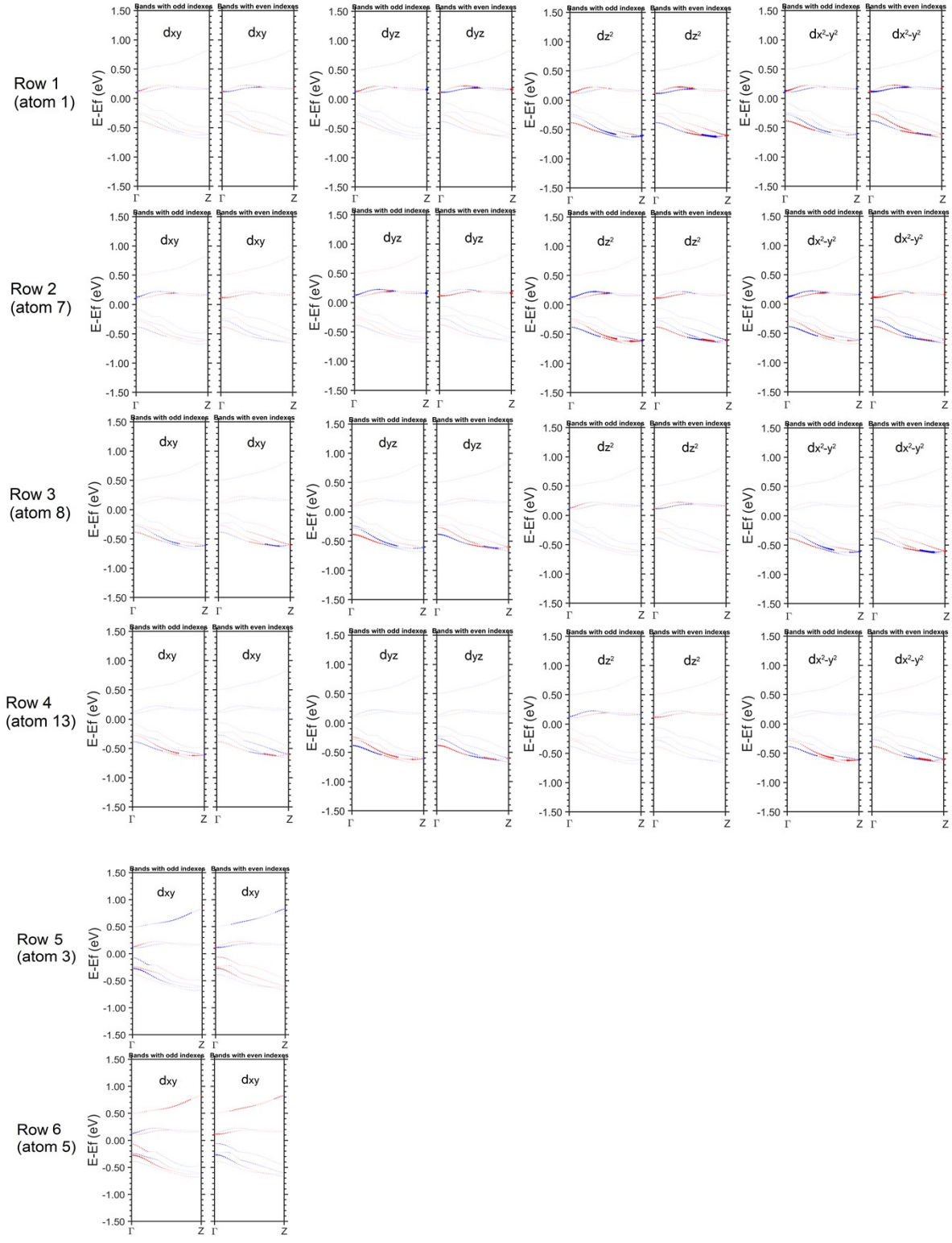

Figure S13. The band structure maps of the d-orbital-decomposed spin-polarization along the y axis for the W atoms in the A13WSe2 nanoribbon under bending curvature radius $R = 6$ Å. Plots are organized in the same way as in Figure S9.

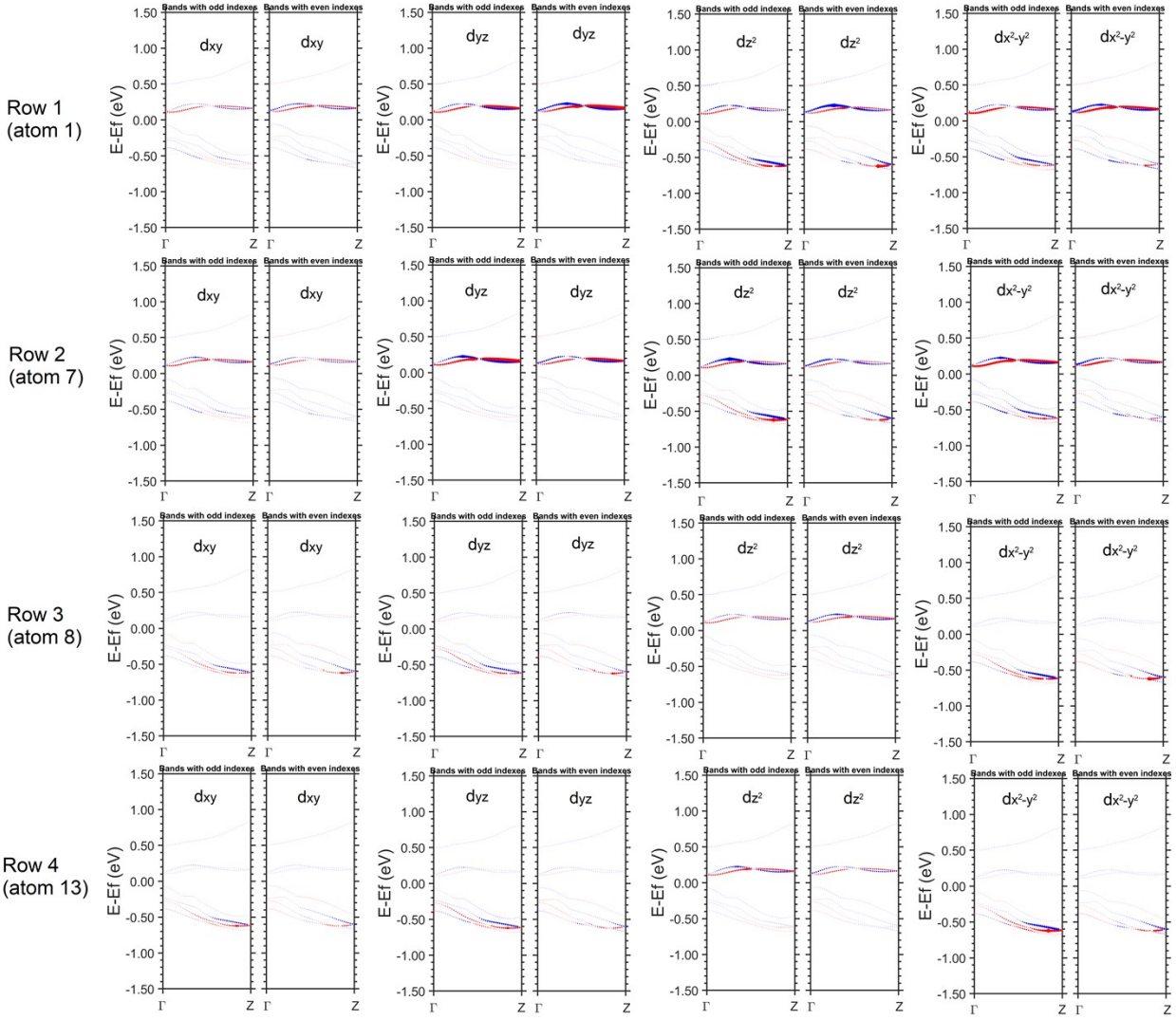

This figure is continued to the next page.

Continued to the previous page.

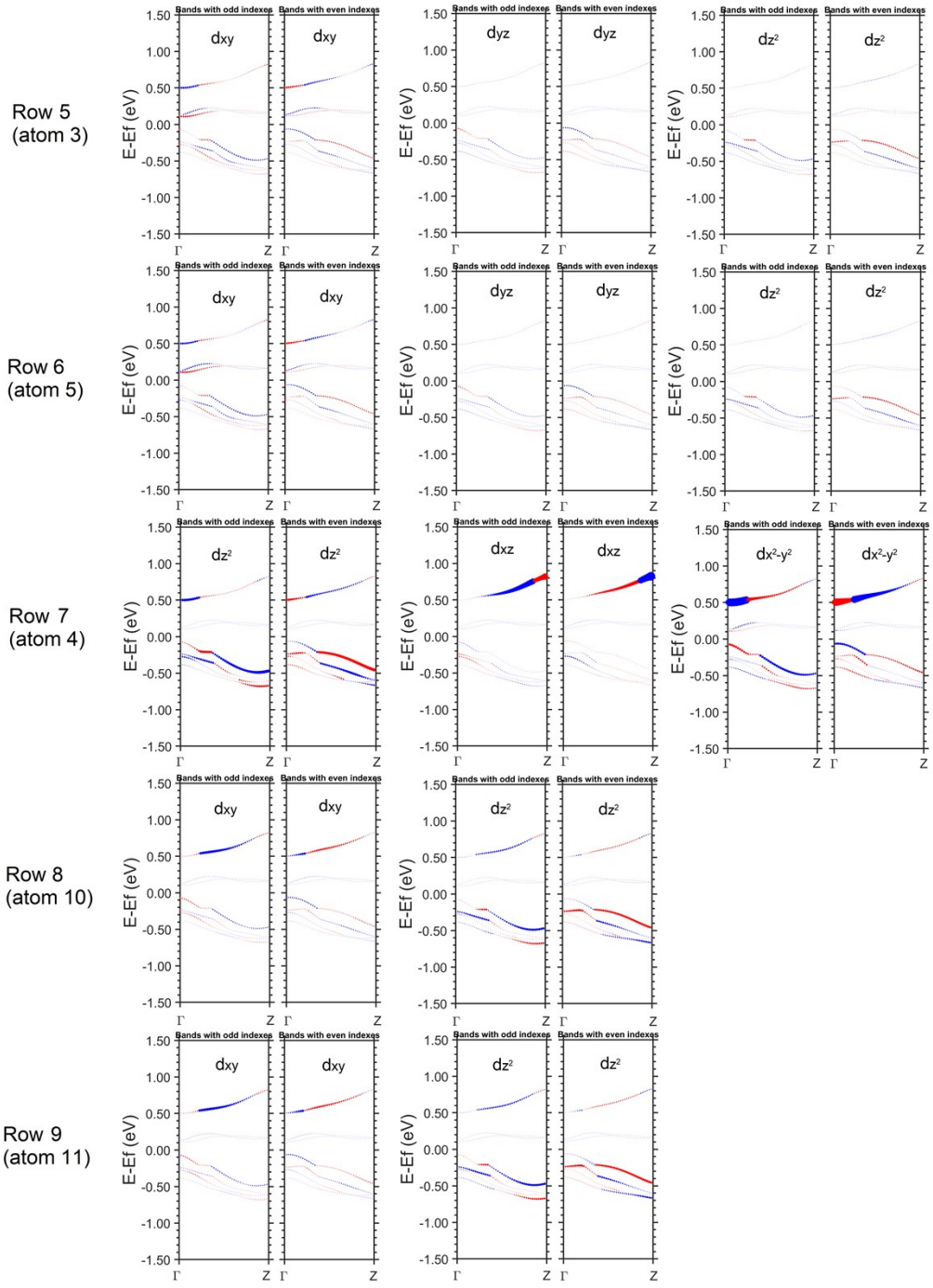

Figure S14. The band structure maps of the d-orbital-decomposed spin-polarization along the x axis for the W atoms in the A13WSe2 nanoribbon under bending curvature radius $R = 6$ Å. The full figure is split, also see the previous page. Plots are organized in the same way as in Figure S9.

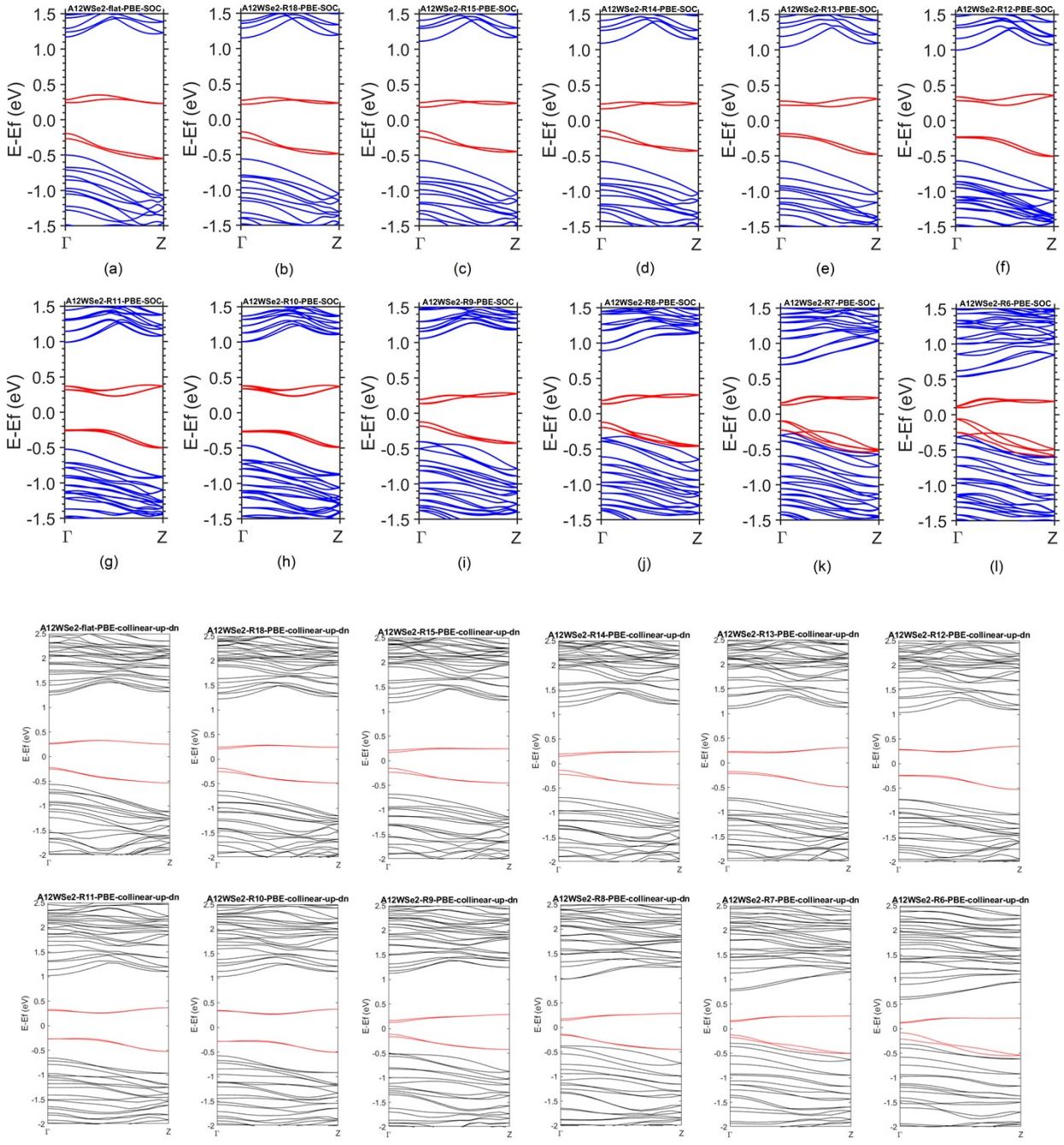

Figure S15. The band structures of the A12WSe2 nanoribbon under different bending radii. The upper panels plot in blue and red curves are for the PBE+SOC results. The lower panels plot in black and red curves are for the PBE without SOC results. See the title on each panel for the bending radius. As can be seen in the band structures with SOC, the flat A12WSe$_2$ also has a direct NEG and a slightly indirect EG. For relatively small ($14\ \text{Å} \le R \le 18\ \text{Å}$) and larger bending ($R \le 9\ \text{Å}$), both NEG and EG of A12WSe$_2$ are direct. However, for intermediate bending radius ($10\ \text{Å} \le R \le 13\ \text{Å}$), A12WSe$_2$ has an indirect EG within the range of $\Gamma - Z$, while its NEG remains direct at Γ.

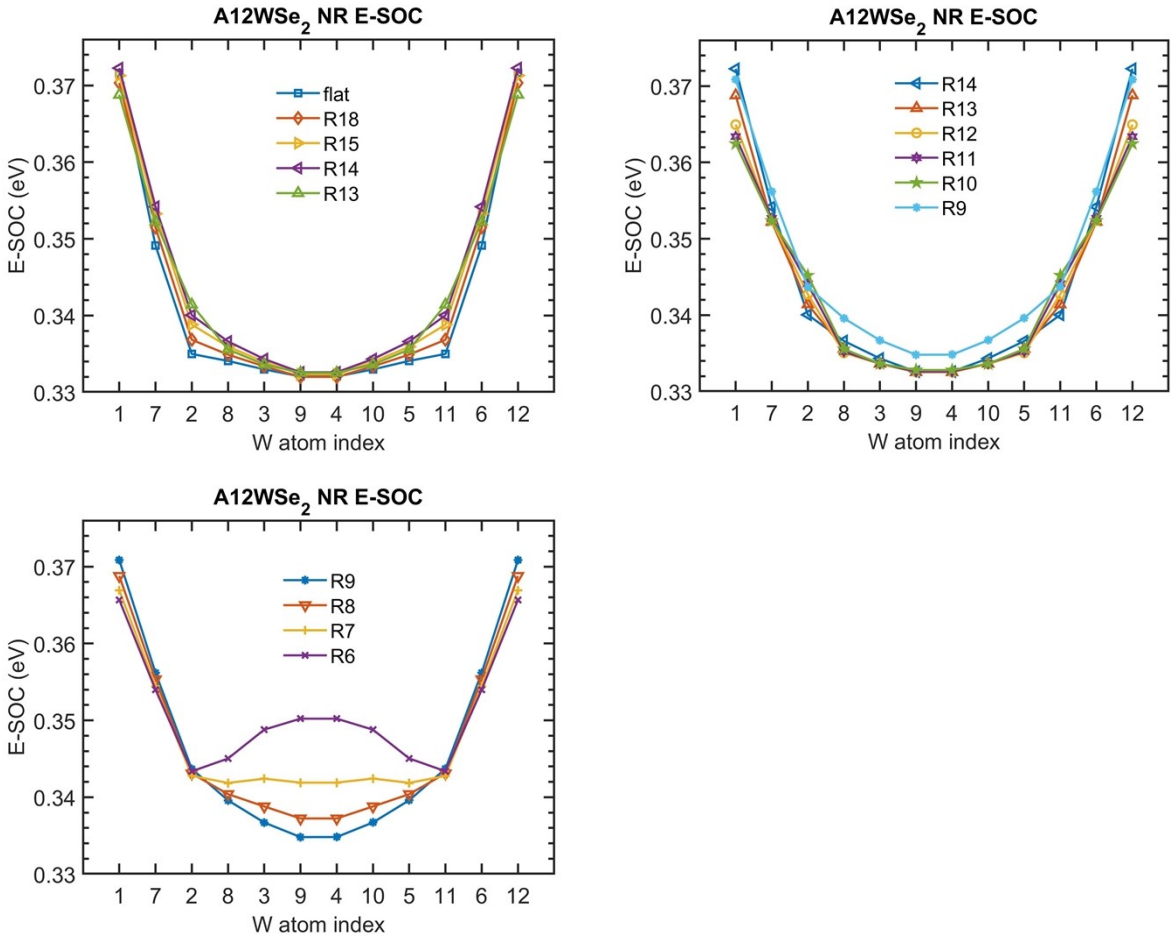

Figure S16. The SOC energy on each metal site in the A12WSe2 nanoribbon under different bending radii.

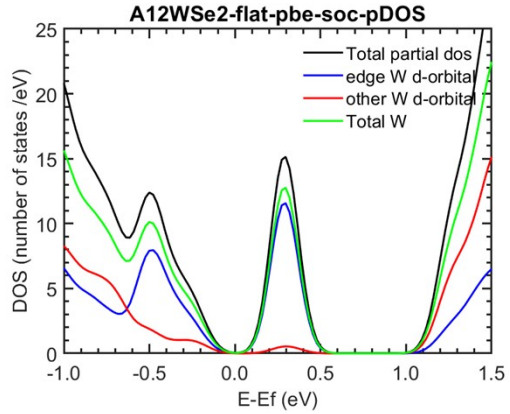

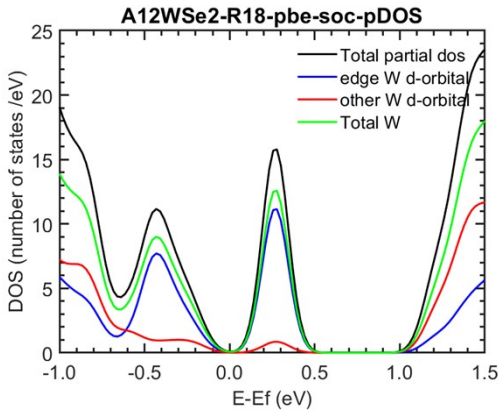

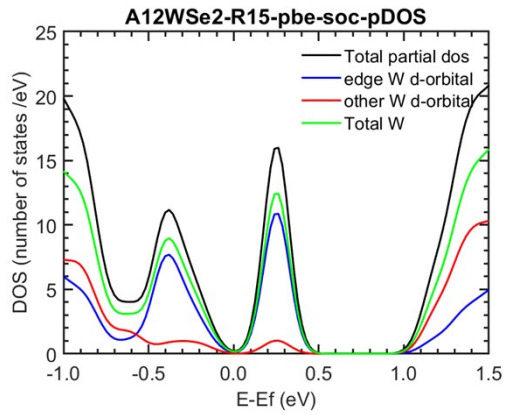

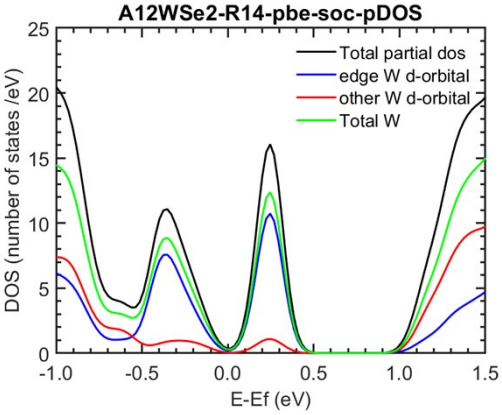

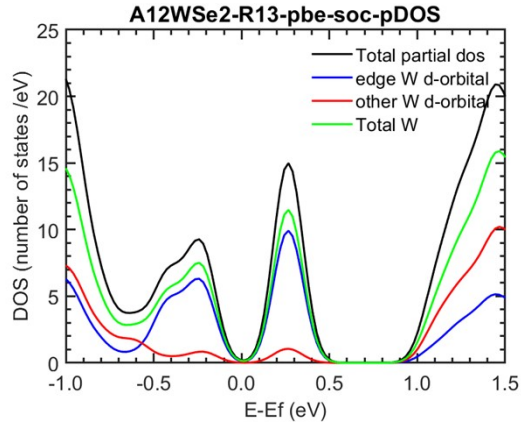

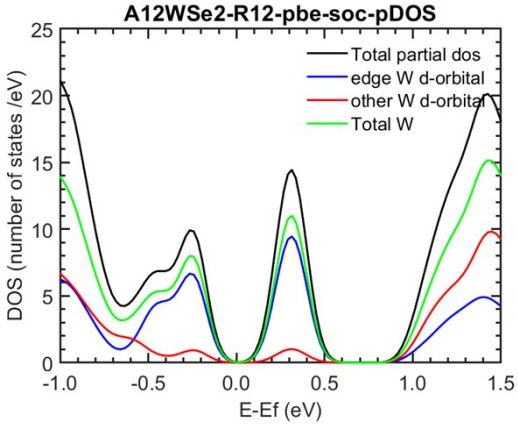

To be continued on the next page.

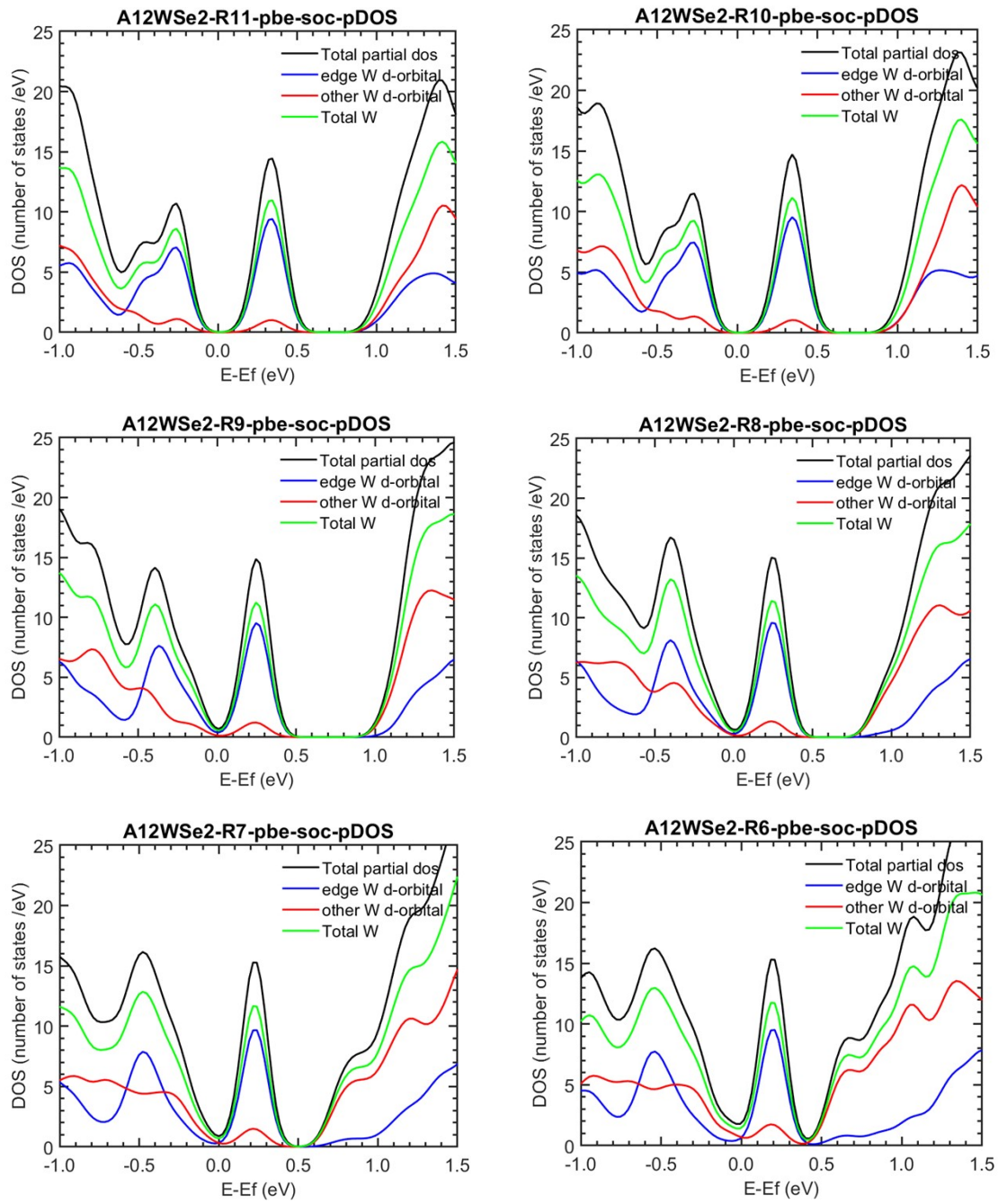

Figure S17. The analysis of the density of states of the A12WSe2 nanoribbon under different bending radii calculated with PBE+SOC. See the title on each panel for the bending radius.

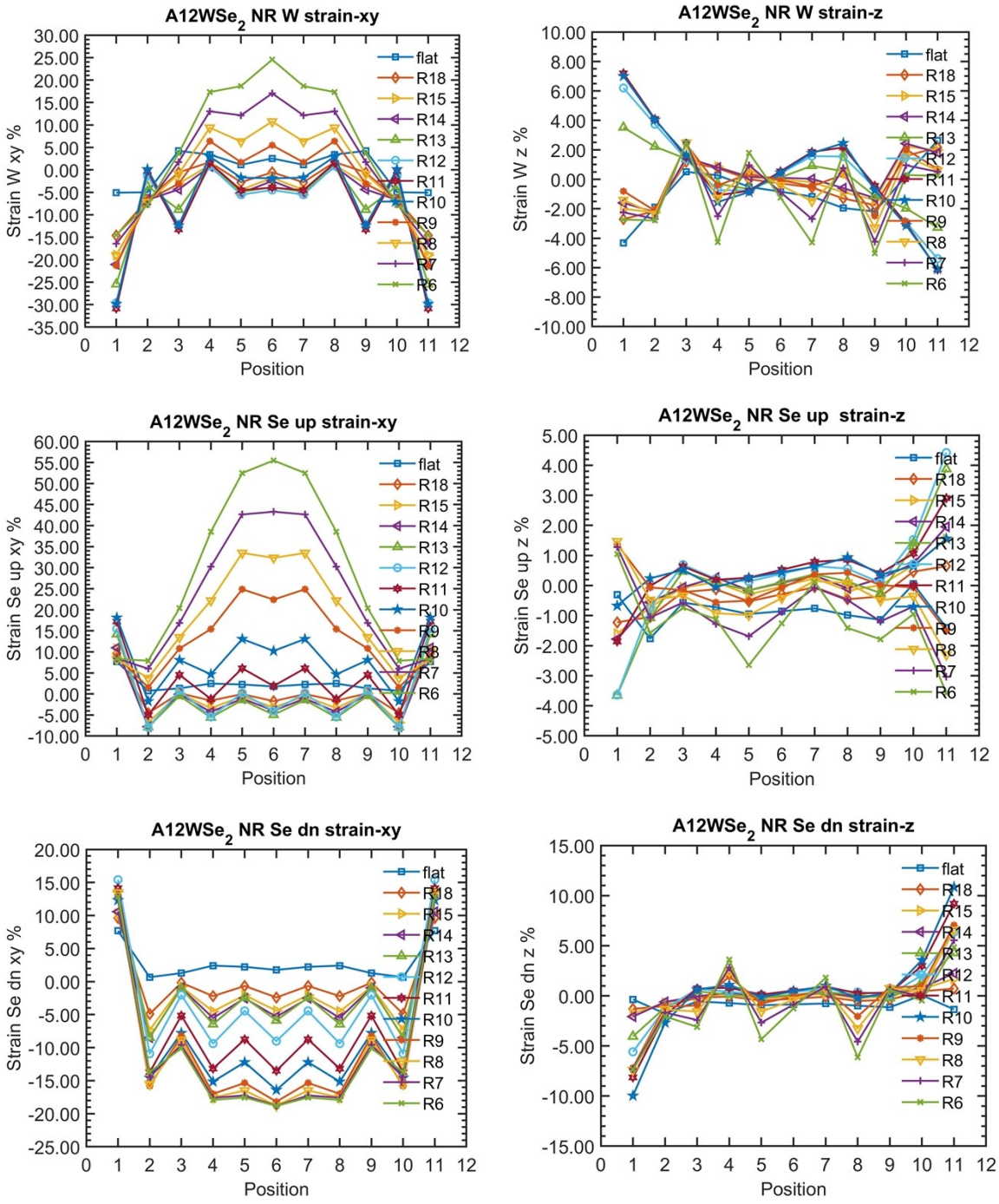

Figure S18. The strains in the A12WSe2 nanoribbon under different bending radii calculated with PBE and the SOC effect included. See the title on each plot for the type of strains.

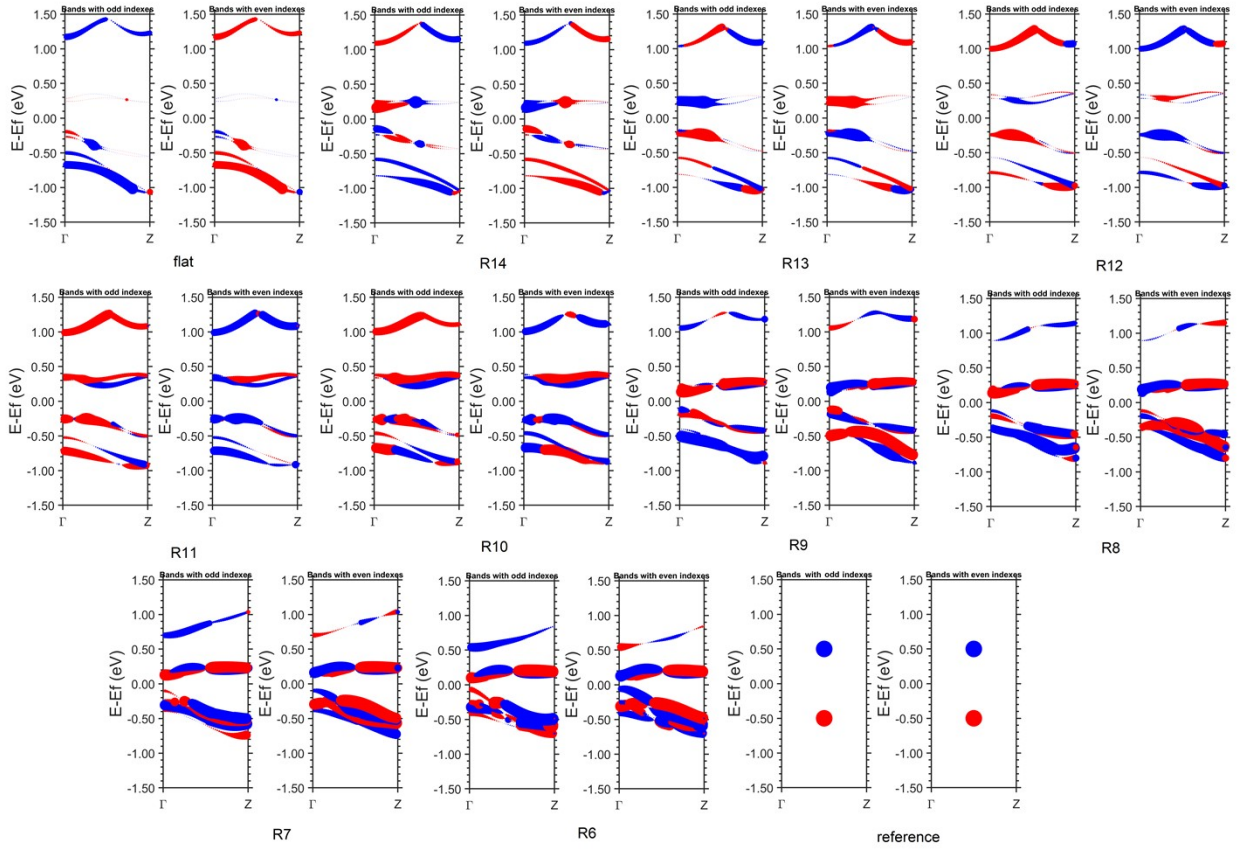

Figure S19. The k point and band resolved spin polarization along the x axis (along the width direction of the nanoribbon) of the A12WSe_2 nanoribbon under different bending curvature radii R calculated with PBE+SOC. In each bending radius panel, the left subplot is for odd number indexed bands, while the right one is for the even number indexed bands. The red (blue) color represents the spin-up (spin-down) spin polarization, with the spin-up (spin-down) points to the negative (positive) direction of the x axis. The magnitude of the magnetic moment (in the unit of Bohr magneton μ_B) at each k point and each band is proportional to the size of the spot. Panel "reference" represents the reference size of the spots with the magnetic moment of 1 μ_B (red) or -1 μ_B (blue).

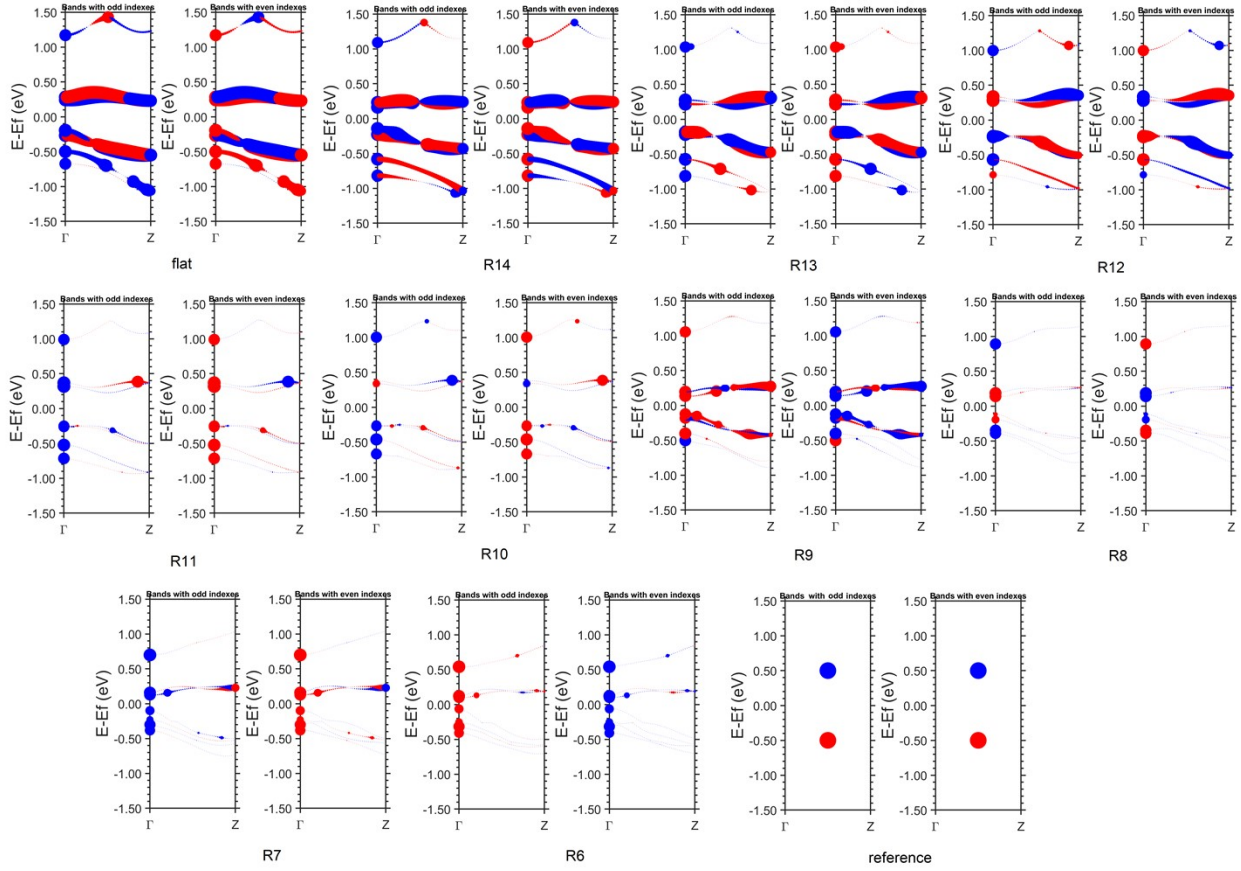

Figure S20. The k point and band resolved spin polarization along the y axis (perpendicular to the plane of the nanoribbon) of the A12WSe$_2$ nanoribbon under different bending curvature radii R calculated with PBE+SOC. In each bending radius panel, the left subplot is for odd number indexed bands, while the right one is for the even number indexed bands. The red (blue) color represents the spin-up (spin-down) spin polarization, with the spin-up (spin-down) points to the positive (negative) direction of the y axis. The magnitude of the magnetic moment (in the unit of Bohr magneton μ_B) at each k point and each band is proportional to the size of the spot. Panel "reference" represents the reference size of the spots with the magnetic moment of 1 μ_B (red) or -1 μ_B (blue).

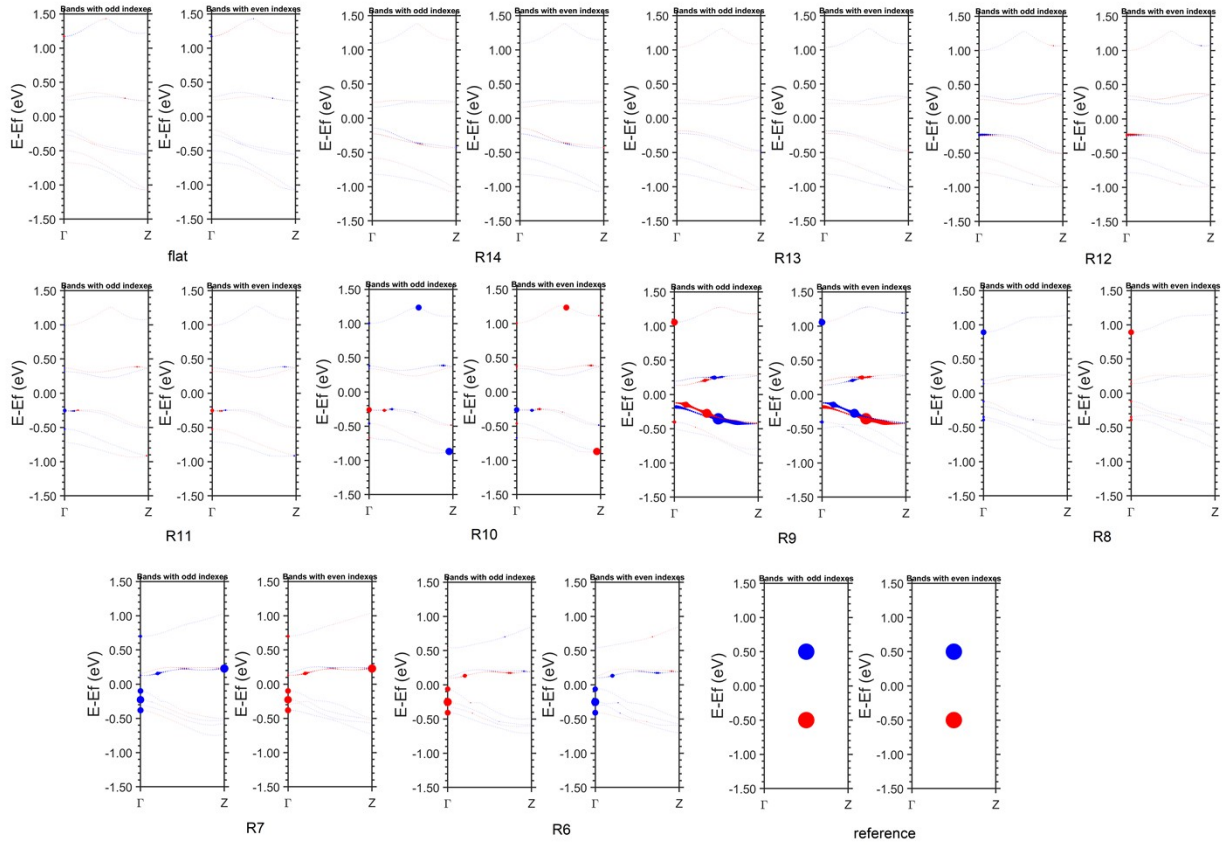

Figure S21. The k point and band resolved spin polarization along the z axis (along the periodical length of the nanoribbon) of the A12WSe_2 nanoribbon under different bending curvature radii R calculated with PBE+SOC. In each bending radius panel, the left subplot is for odd number indexed bands, while the right one is for the even number indexed bands. The red (blue) color represents the spin-up (spin-down) spin polarization, with the spin-up (spin-down) points to the negative (positive) direction of the z axis. The magnitude of the magnetic moment (in the unit of Bohr magneton μ_B) at each k point and each band is proportional to the size of the spot. Panel "reference" represents the reference size of the spots with the magnetic moment of 1 μ_B (red) or -1 μ_B (blue).

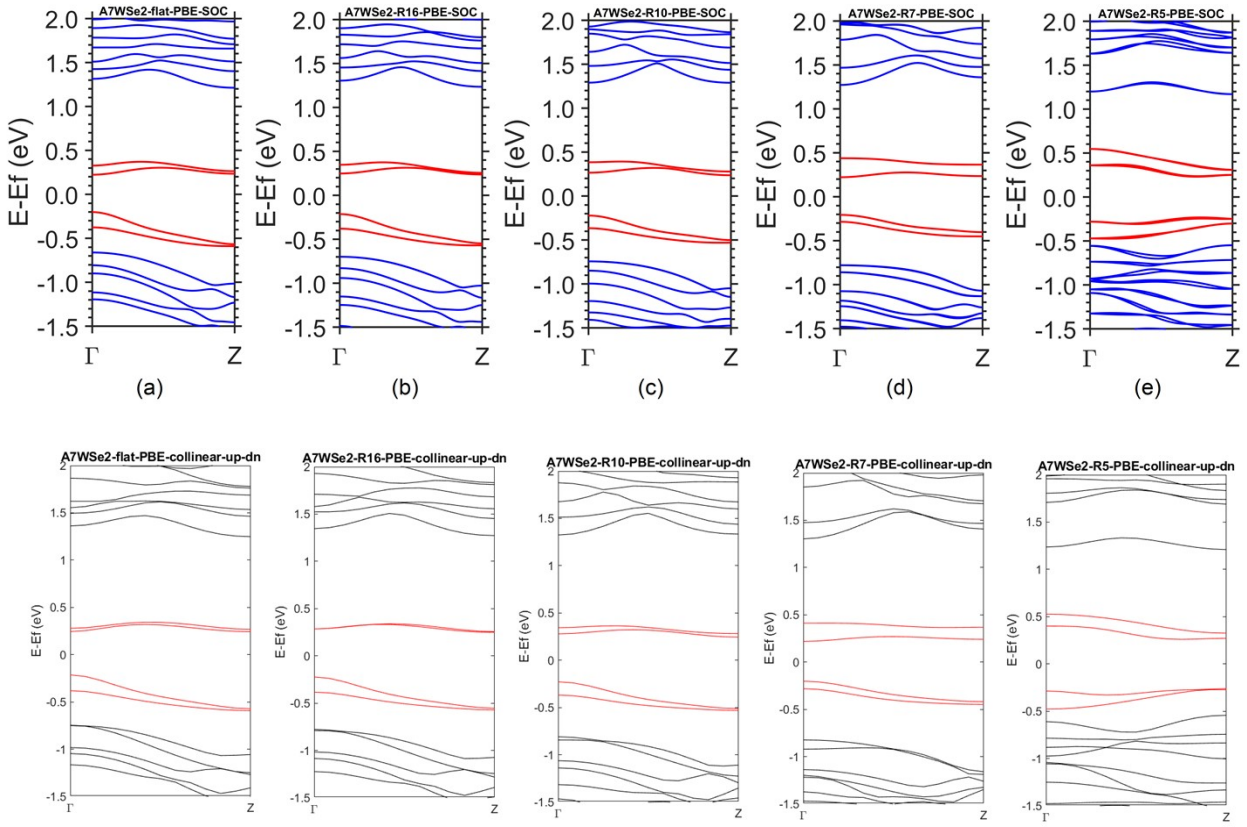

Figure S22. The band structures of the A7WSe2 nanoribbon under different bending radii. The upper panels plot in blue and red curves are for the PBE+SOC results. The lower panels plot in black and red curves are for the PBE without SOC results. See the title on each panel for the bending radius. As can be seen in the band structures with SOC, its NEG is slightly indirect generally, while for bending at $R = 10$ Å and $R = 7$ Å, it becomes slightly direct. Its EG is generally slightly direct (or slightly indirect) between k points Γ and Z, while at the large bending curvature $R = 5$ Å, the EG of A7WSe$_2$ is almost direct at a k point along line $\Gamma - Z$ and close to Z.

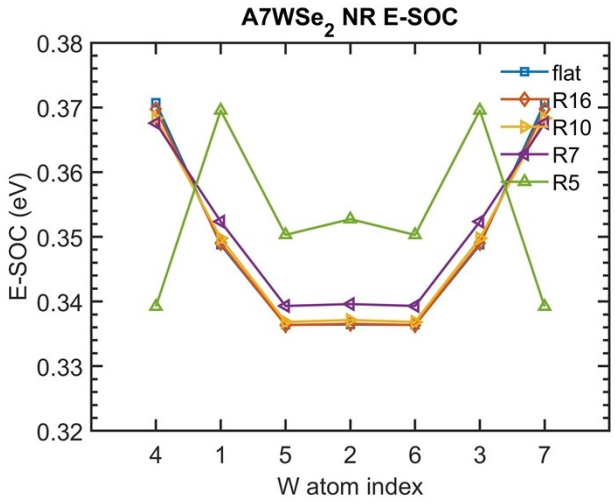

Figure S23. The SOC energy on each metal site in the A7WSe2 nanoribbon under different bending radii.

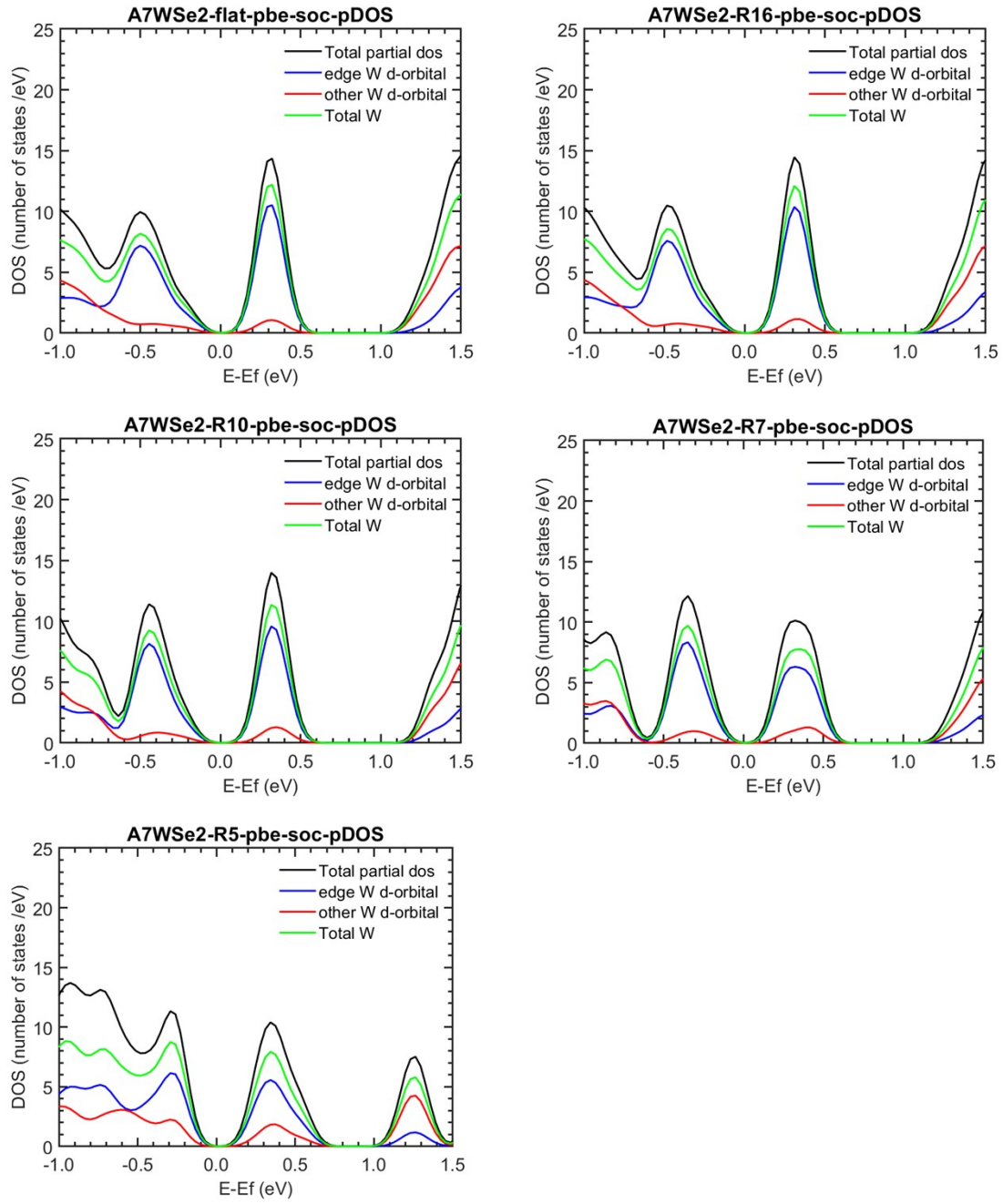

Figure S24. The analysis of the density of states of the A7WSe2 nanoribbon under different bending radii calculated with PBE+SOC. See the title on each panel for the bending radius.

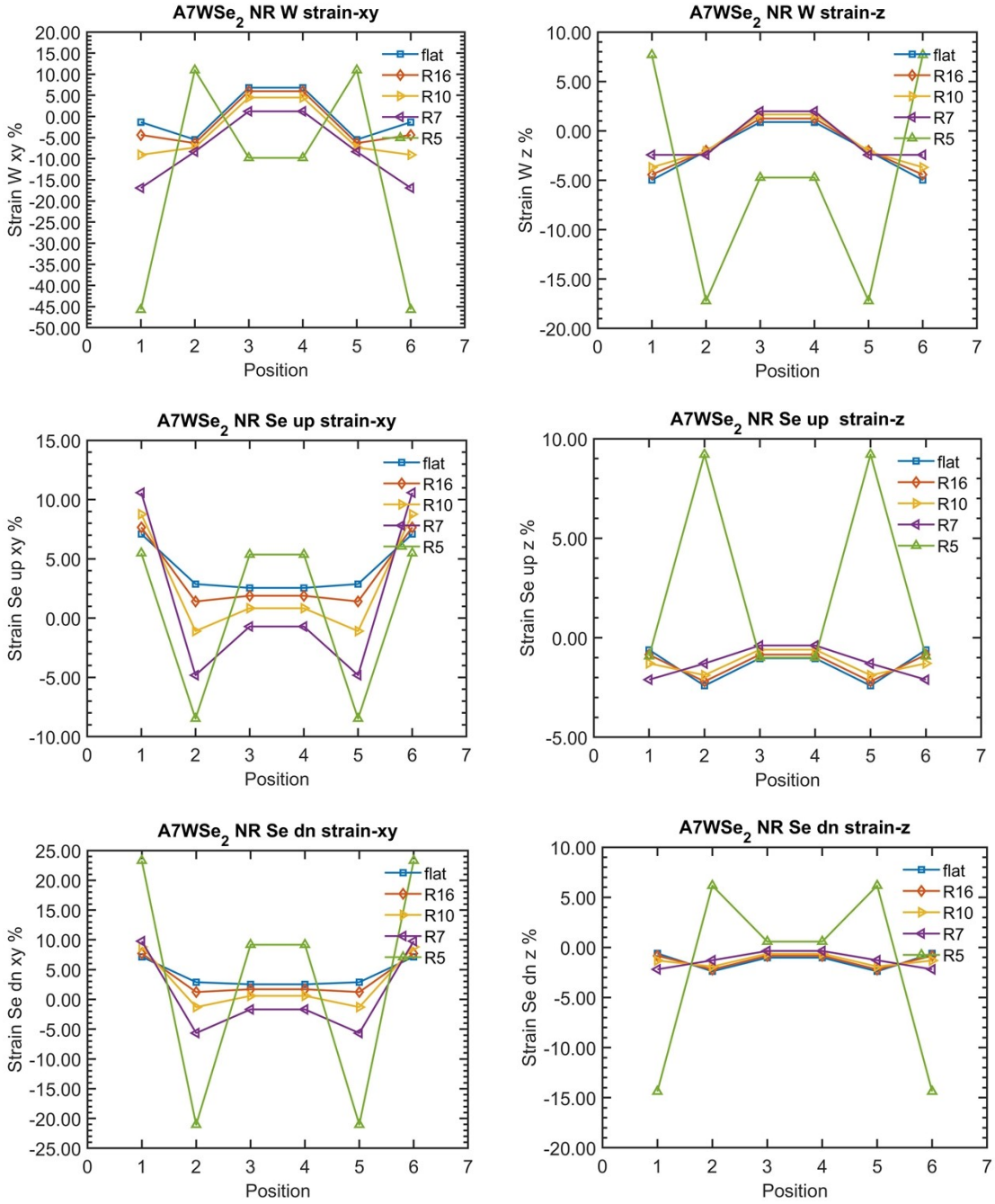

Figure S25. The strains in the A7WSe2 nanoribbon under different bending radii calculated with PBE and the SOC effect included. See the title on each plot for the type of strains.

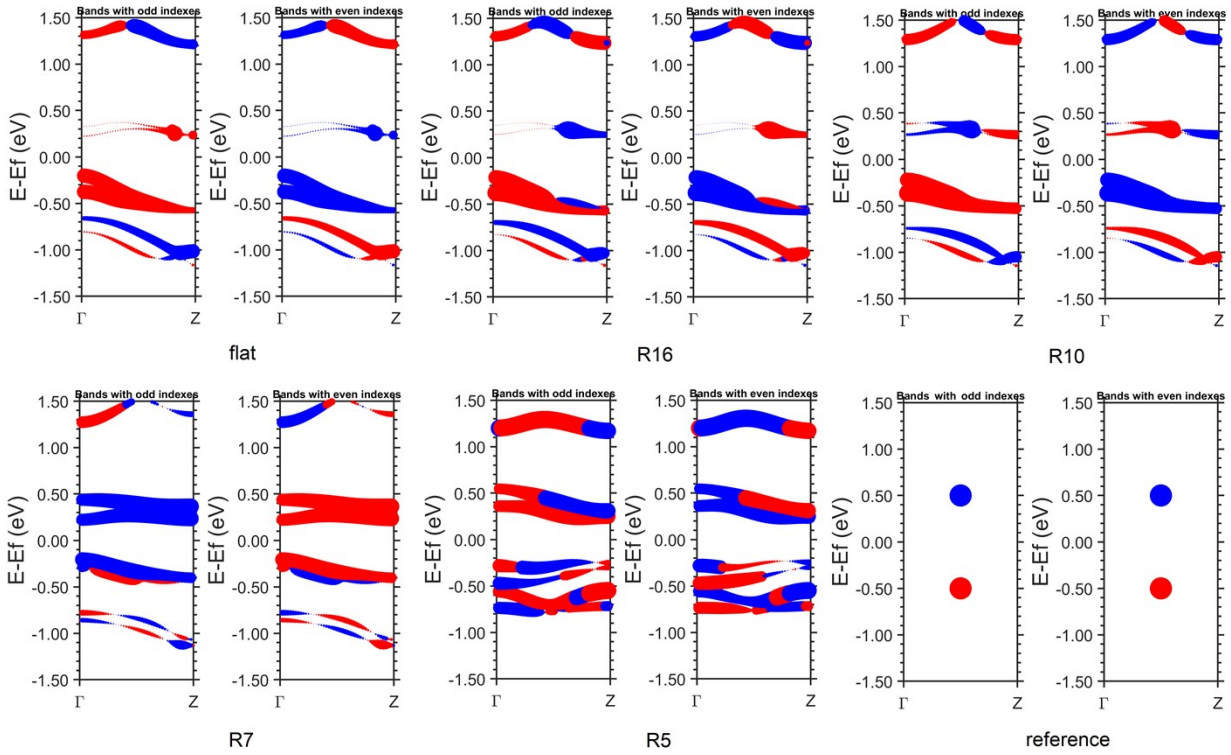

Figure S26. The k point and band resolved spin polarization along the x axis (along the width direction of the nanoribbon) of the A7WSe$_2$ nanoribbon under different bending curvature radii R calculated with PBE+SOC. In each bending radius panel, the left subplot is for odd number indexed bands, while the right one is for the even number indexed bands. The red (blue) color represents the spin-up (spin-down) spin polarization, with the spin-up (spin-down) points to the negative (positive) direction of the x axis. The magnitude of the magnetic moment (in the unit of Bohr magneton μ_B) at each k point and each band is proportional to the size of the spot. Panel "reference" represents the reference size of the spots with the magnetic moment of 1 μ_B (red) or -1 μ_B (blue).

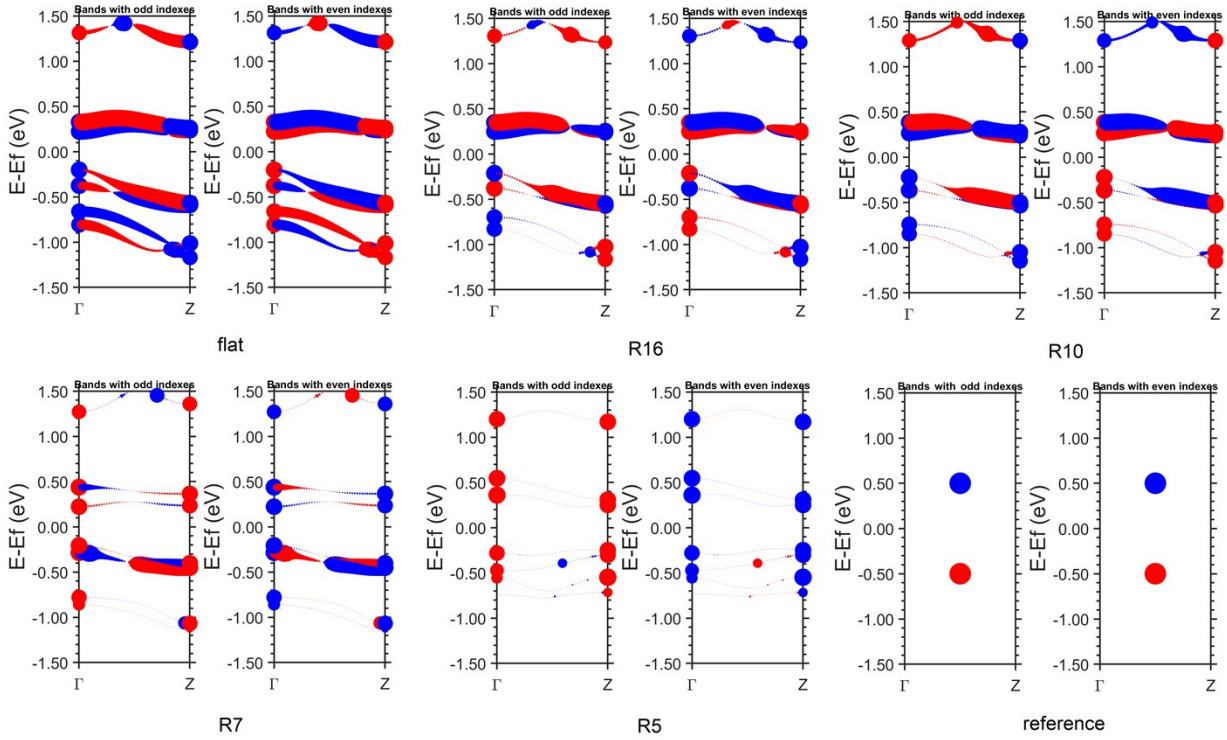

Figure S27. The k point and band resolved spin polarization along the y axis (perpendicular to the plane of the nanoribbon) of the A7WSe$_2$ nanoribbon under different bending curvature radii R calculated with PBE+SOC. In each bending radius panel, the left subplot is for odd number indexed bands, while the right one is for the even number indexed bands. The red (blue) color represents the spin-up (spin-down) spin polarization, with the spin-up (spin-down) points to the positive (negative) direction of the y axis. The magnitude of the magnetic moment (in the unit of Bohr magneton μ_B) at each k point and each band is proportional to the size of the spot. Panel "reference" represents the reference size of the spots with the magnetic moment of 1 μ_B (red) or -1 μ_B (blue).

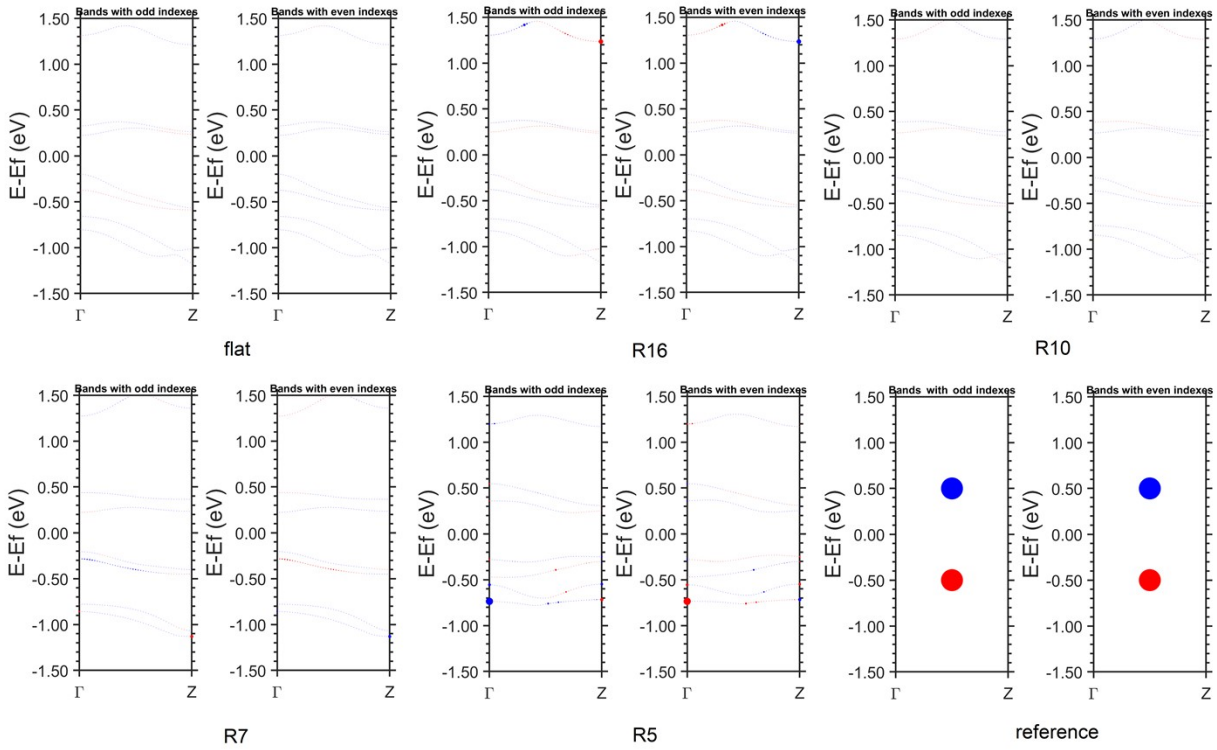

Figure S28. The k point and band resolved spin polarization along the z axis (along the periodical length of the nanoribbon) of the A7WSe$_2$ nanoribbon under different bending curvature radii R calculated with PBE+SOC. In each bending radius panel, the left subplot is for odd number indexed bands, while the right one is for the even number indexed bands. The red (blue) color represents the spin-up (spin-down) spin polarization, with the spin-up (spin-down) points to the negative (positive) direction of the z axis. The magnitude of the magnetic moment (in the unit of Bohr magneton μ_B) at each k point and each band is proportional to the size of the spot. Panel "reference" represents the reference size of the spots with the magnetic moment of 1 μ_B (red) or -1 μ_B (blue).

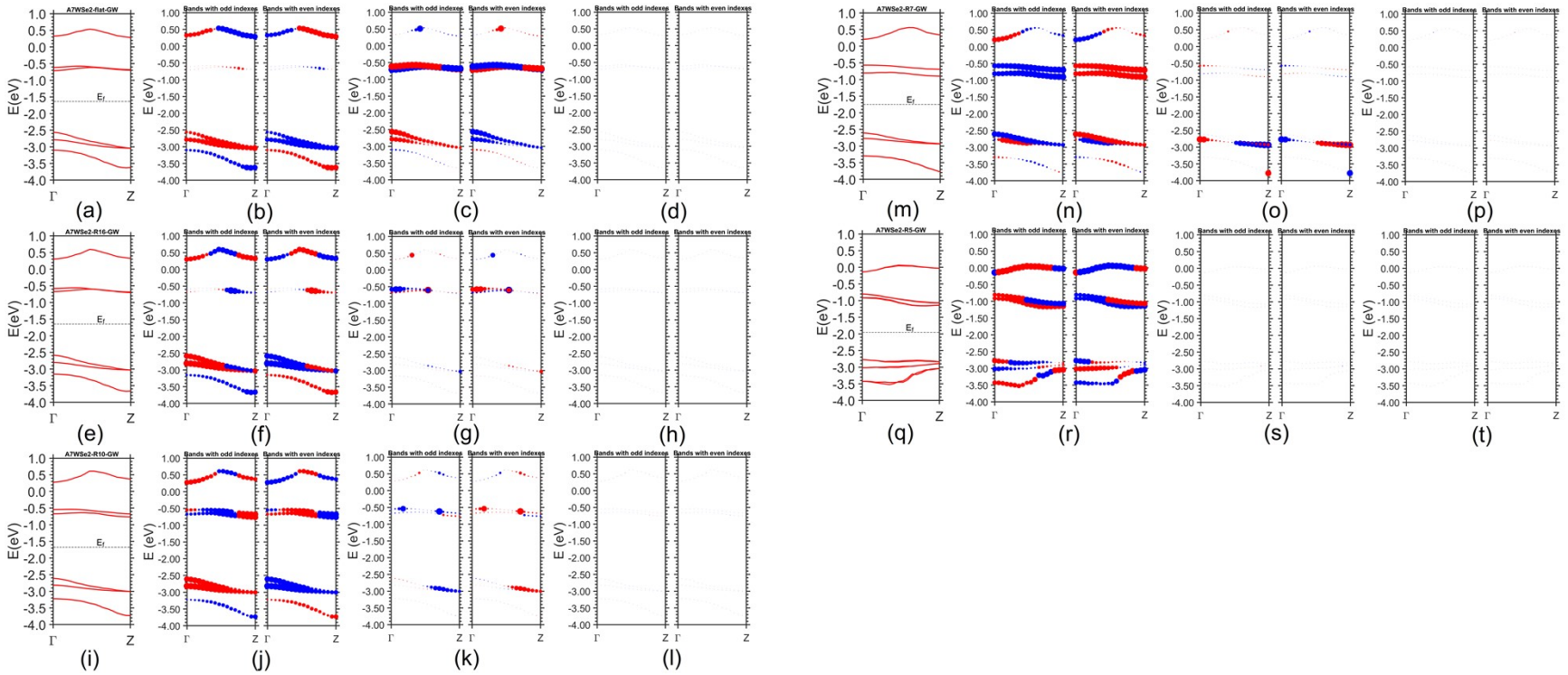

Figure S29. The G_0W_0 band structures and k point and band resolved spin polarizations of the A7WSe2 nanoribbon under different bending conditions. Panels (a), (b), (c) and (d) are the G_0W_0 band structure, spin polarization along axis x, spin polarization along axis y, and spin polarization along axis z, respectively, for the flat nanoribbon. In panels (b)-(d), the odd number indexed bands are plot on the left side and the even numbered ones are on the right side with the same energy scale, for clarity. Panels (e)-(h) are for bending radius $R = 16$ Å. Panels (i)-(l) are for bending radius $R = 10$ Å. Panels (m)-(p) are for bending radius $R = 7$ Å. Panels (q)-(t) are for bending radius $R = 5$ Å. The figure panels in each set of radii are arranged in the similar way. The dashed horizontal lines in (a), (e), (i), (m) and (q) represent the Fermi level. The directions to which a spin-up (or a spin-down) polarization points in the three spatial x, y and z axes are the same as those defined in Figures S26, S27, and S28.

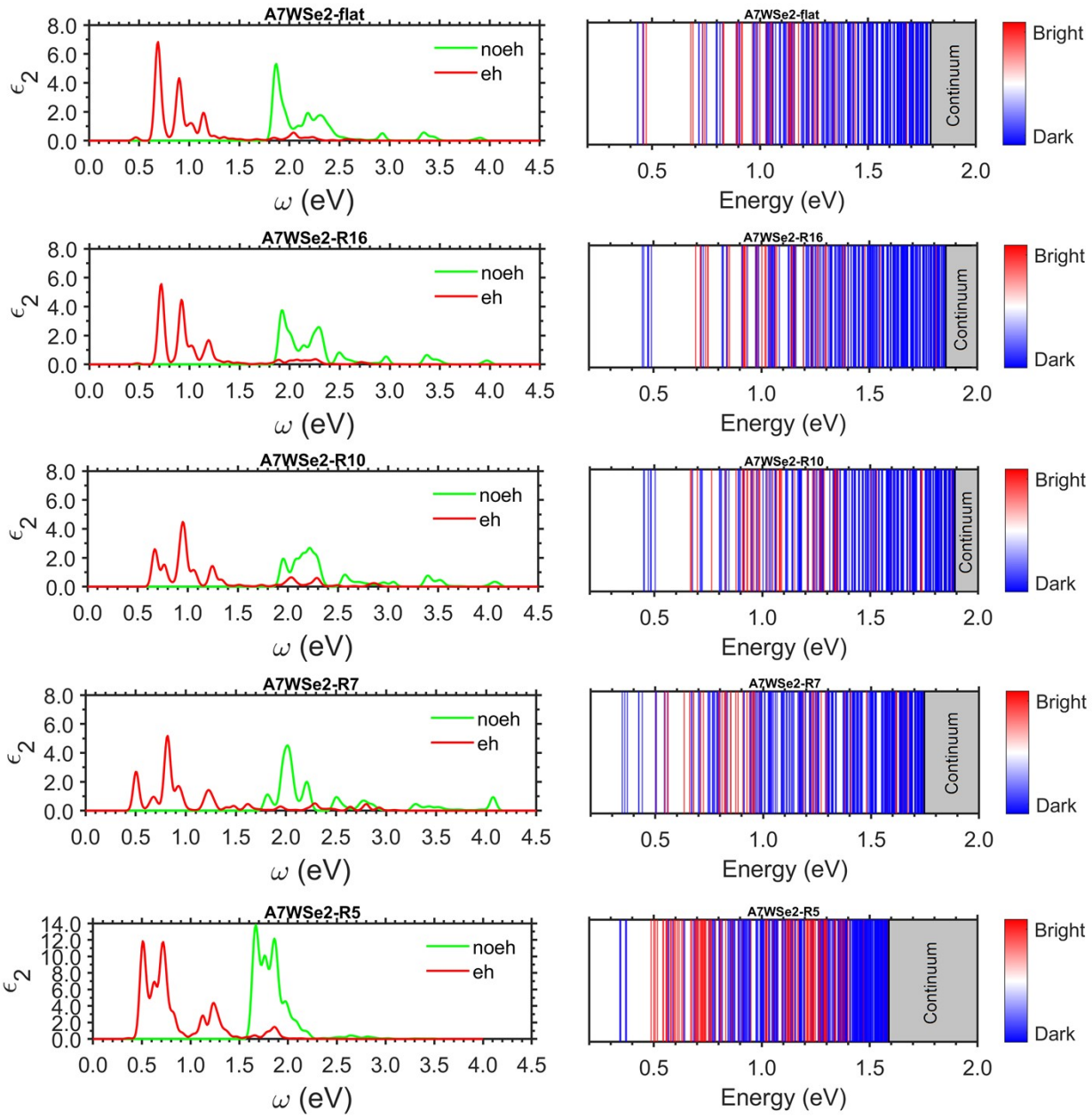

Figure S30. The optical absorption spectra and the corresponding exciton spectra of A7WSe$_2$ nanoribbon under different bending radii. The optical absorption spectra are plotted as the imaginary part of the dielectric function as a function of photon energy. Red curves represent the GW+BSE results with electron-hole (eh) interactions and the green ones are for the results without eh (noeh) interactions, both with constant broadening of 28 meV. The exciton spectra show the energy positions of exciton states. Bright (dark) exciton states are represented by red (blue) lines.

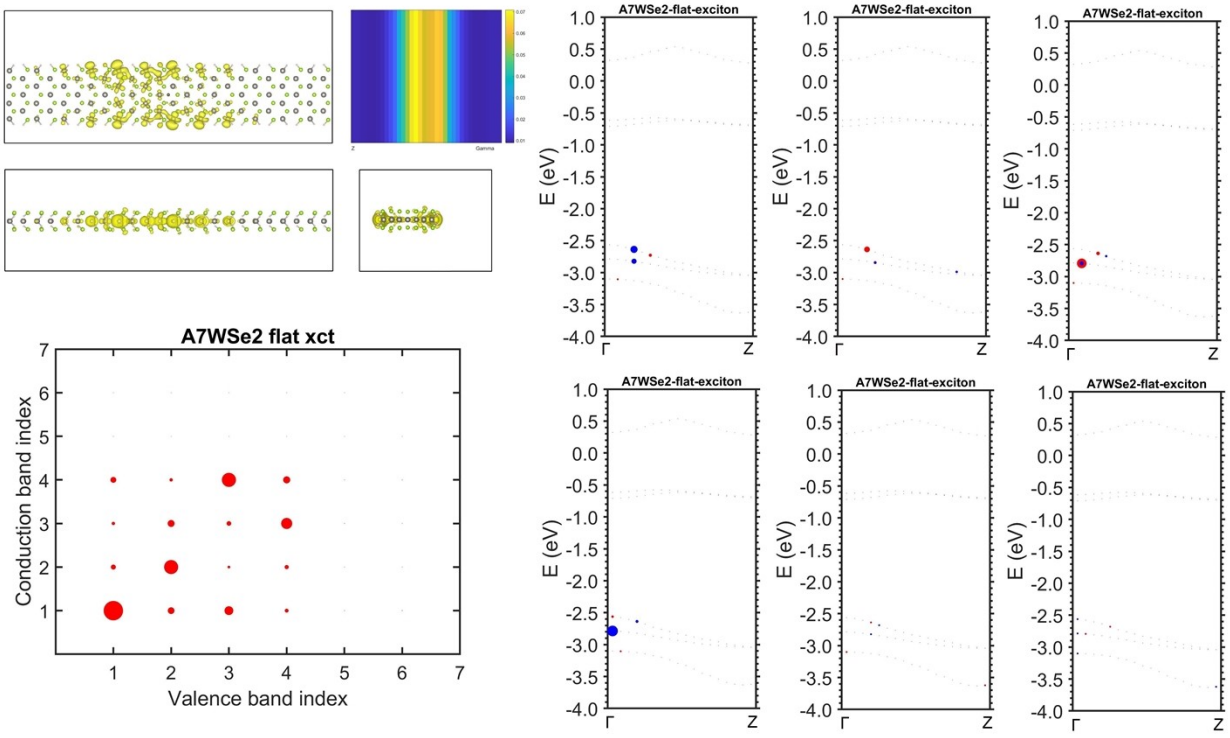

Figure S31. The bright exciton at the energy of 0.90 eV of the flat A7WSe2 nanoribbon. All the subplots are plotted and arranged in the same way as in Figure 7 in the main text.

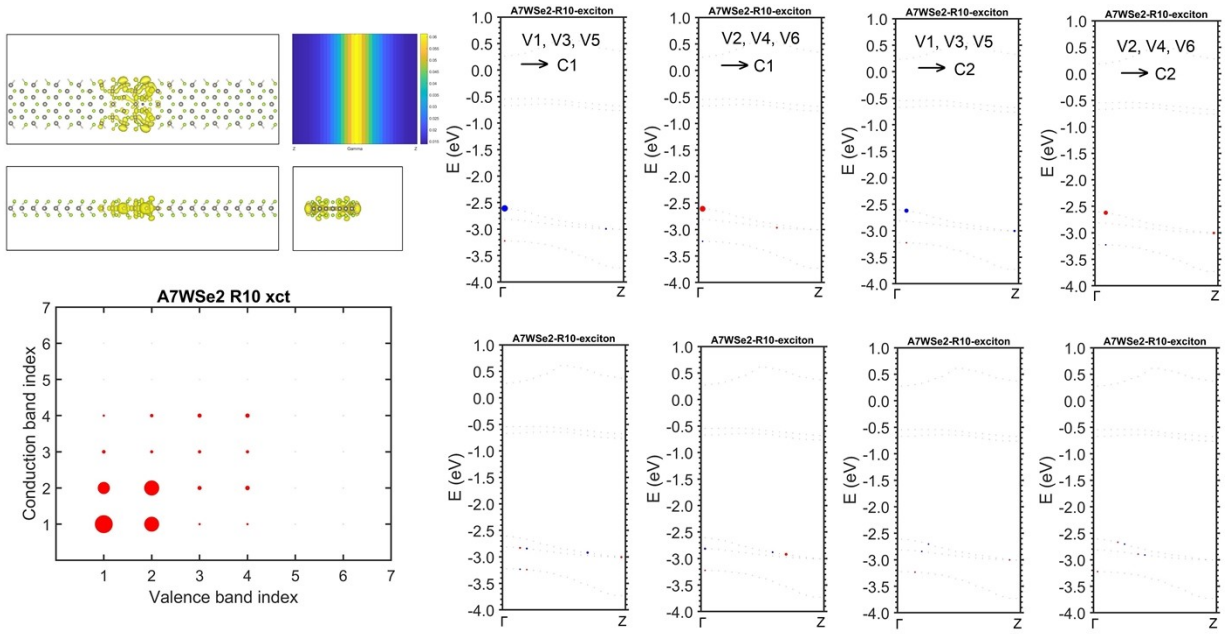

Figure S32. The dark exciton at the energy of 0.45 eV of the A7WSe2 nanoribbon at $R = 10$ Å. The five subplots on the left side are plotted and arranged in the same way as in Figure 7 in the main text. For the eight subplots on the right side, the four subplots in the upper row are for the contributions from the V1, V3, V5 valence bands to the conduction band C1, the V2, V4, V6 valence bands to the conduction band C1, the V1, V3, V5 valence bands to the conduction band C2, and the V2, V4, V6 valence bands to the conduction band C2, respectively. The four subplots in the lower row, from left to right, are for the transitions from all the valence bands (V1-V6) to C3, C4, C5, and C6, respectively.

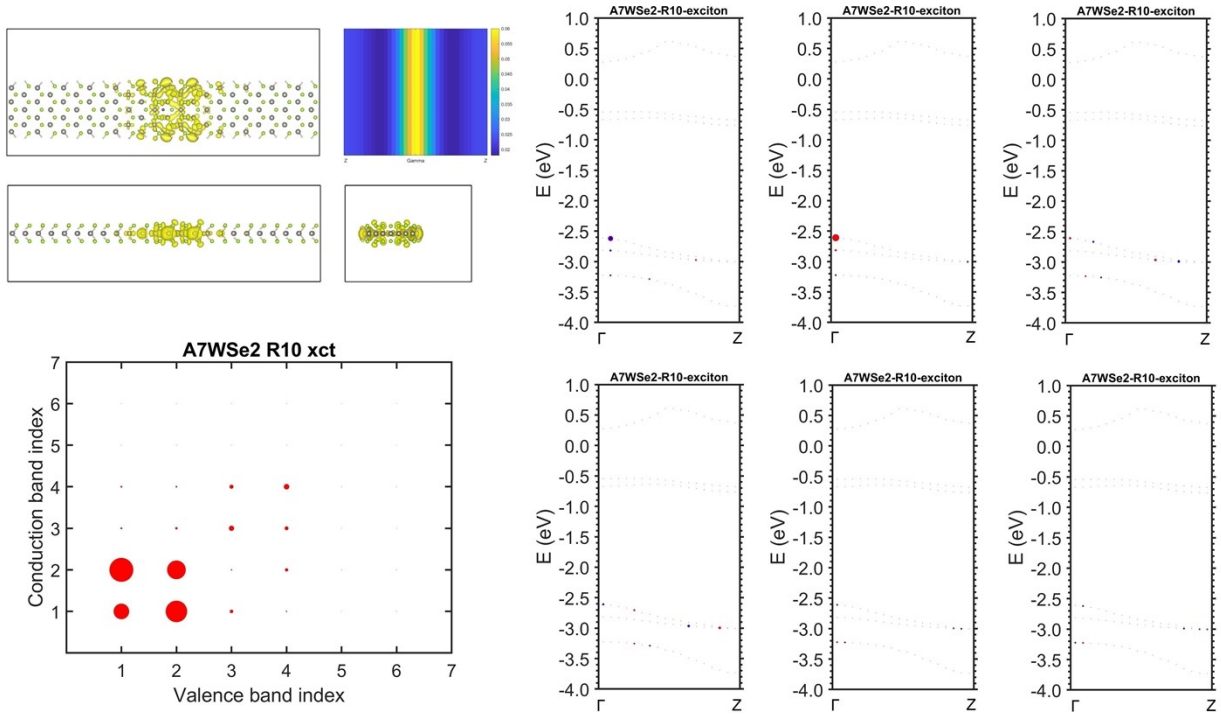

Figure S33. The bright exciton at the energy of 0.67 eV of the A7WSe2 nanoribbon at $R = 10$ Å. All the subplots are plotted and arranged in the same way as in Figure 7 in the main text.

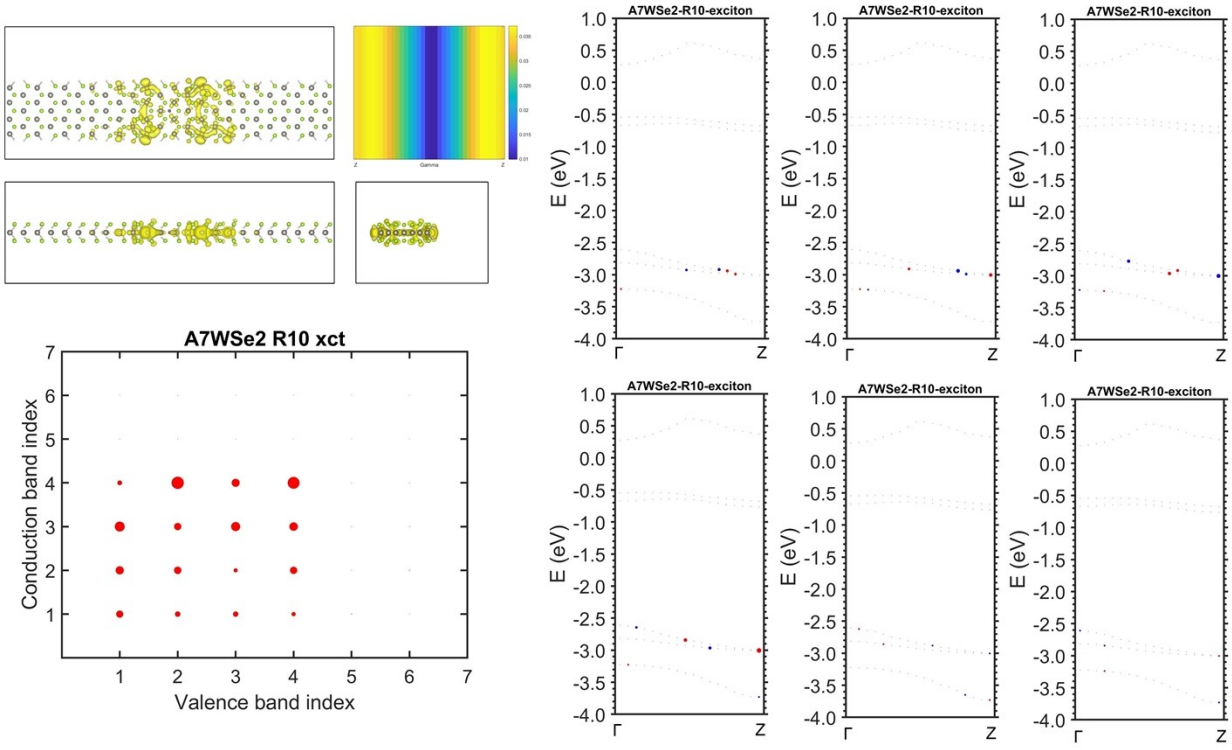

Figure S34. The bright exciton at the energy of 0.93 eV of the A7WSe2 nanoribbon at $R = 10$ Å. All the subplots are plotted and arranged in the same way as in Figure 7 in the main text.

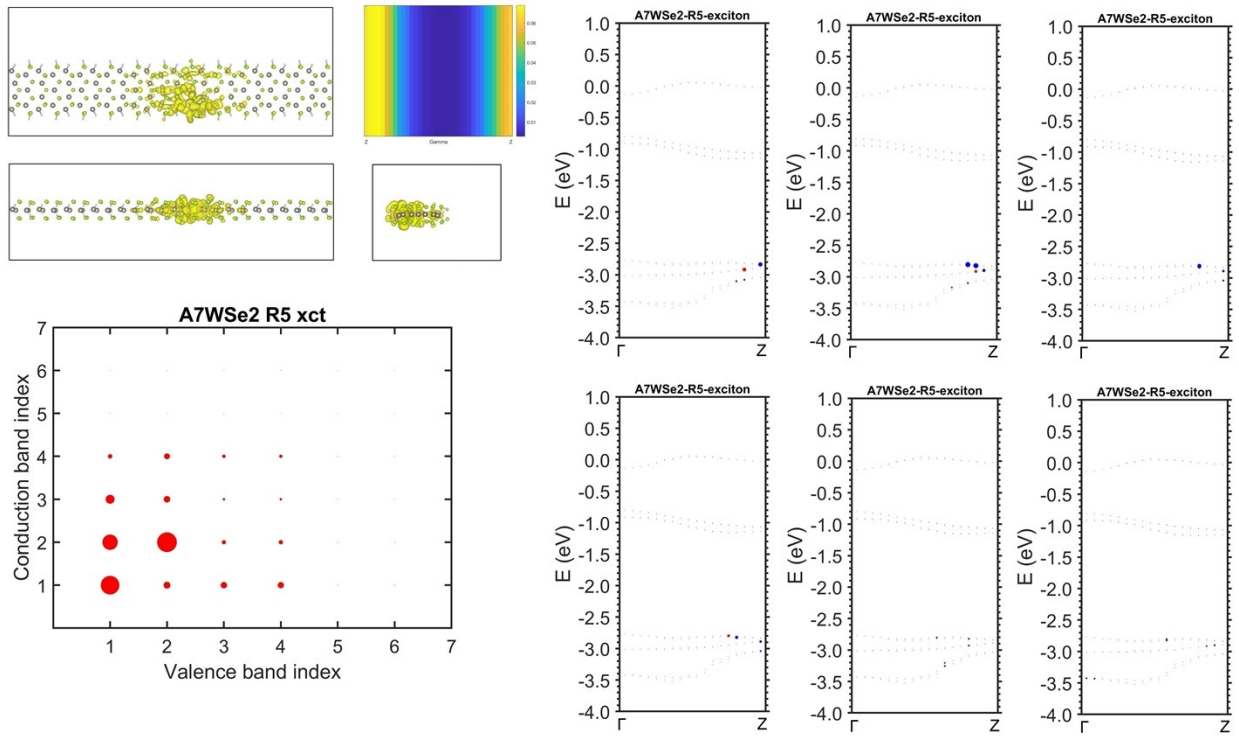

Figure S35. The dark exciton at the energy of 0.34 eV of the A7WSe2 nanoribbon at $R = 5$ Å. All the subplots are plotted and arranged in the same way as in Figure 7 in the main text.

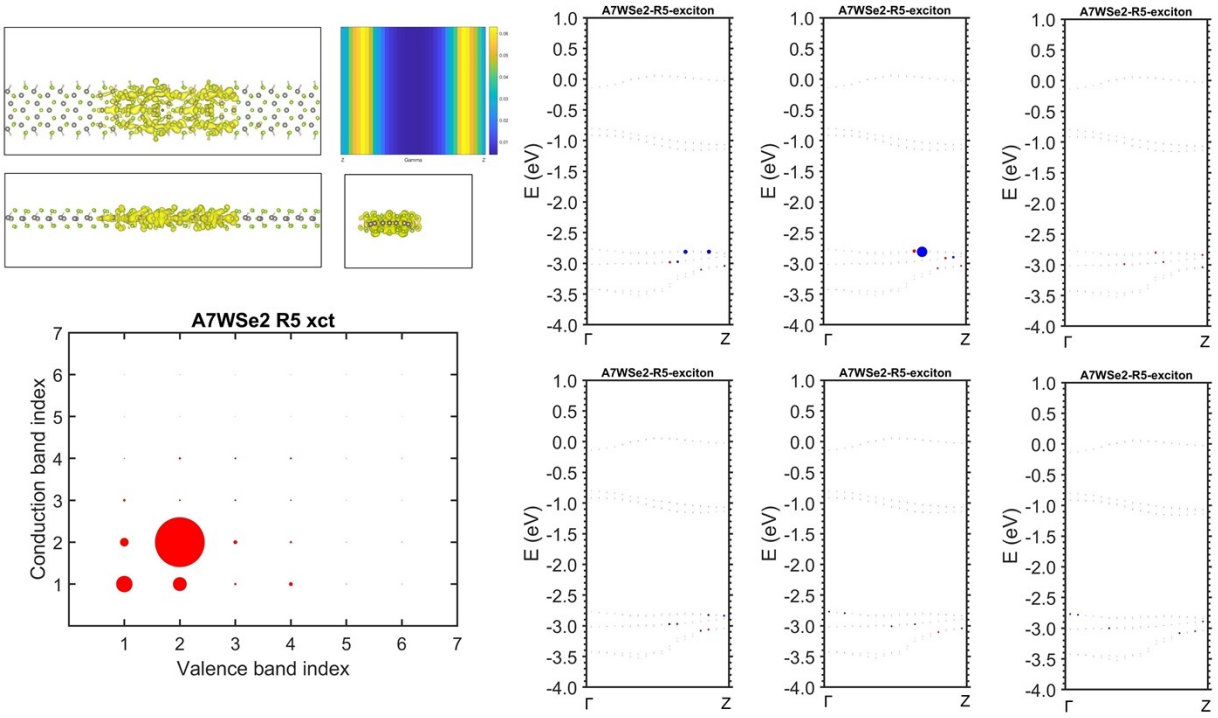

Figure S36. The bright exciton at the energy of 0.52 eV of the A7WSe2 nanoribbon at $R = 5$ Å. All the subplots are plotted and arranged in the same way as in Figure 7 in the main text.

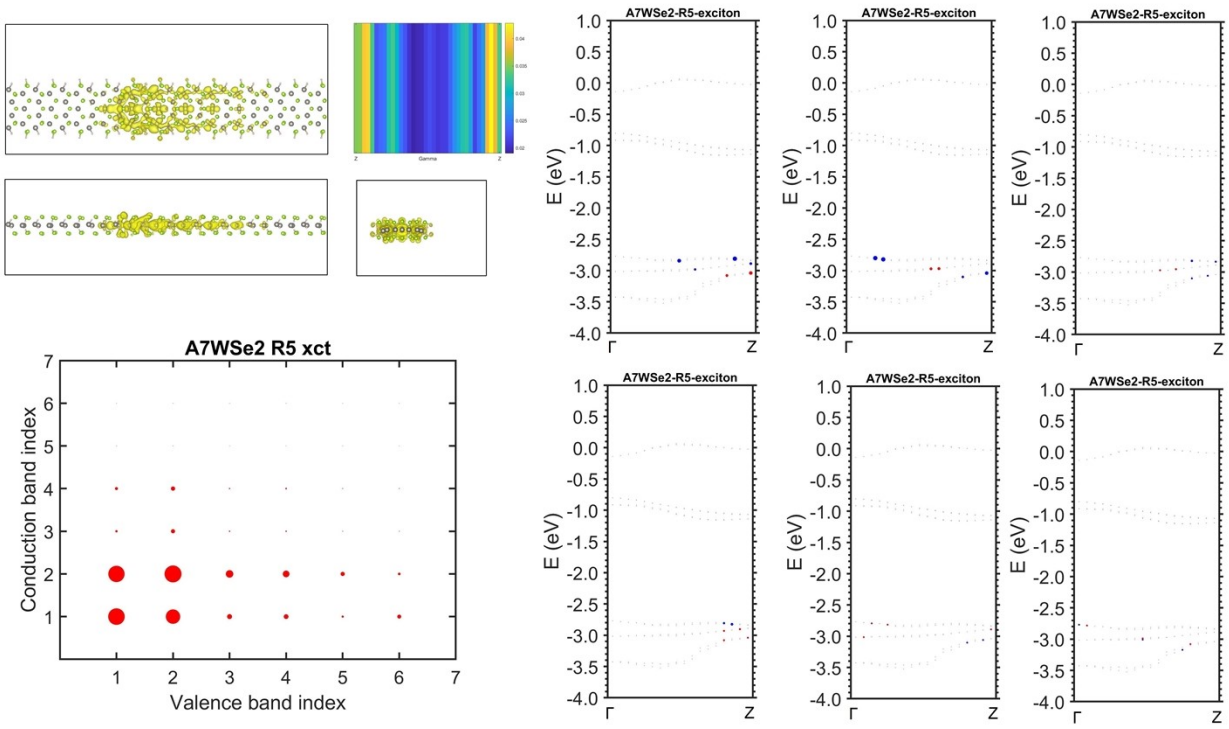

Figure S37. The bright exciton at the energy of 0.70 eV of the A7WSe2 nanoribbon at $R = 5$ Å. All the subplots are plotted and arranged in the same way as in Figure 7 in the main text.

Note 3. Convergence test of optical absorption spectrum

For GW quasiparticle energy, we choose the k grid by comparison with that in Ref. 2, where a k-grid of $12 \times 12 \times 1$ is used for GW quasiparticle energy, equivalent to a distance of $0.026/\text{Å}$ between two adjacent k points in vector a (or b) direction, see Table I in Ref. 2 . This leads to a converged quasiparticle gap within 0.1 eV. We used a k-grid of $1 \times 1 \times 12$ for GW quasiparticle energy for our nanoribbon, and this is equivalent to a distance of $0.015/\text{Å}$ between two adjacent k points in vector c (the ribbon length) direction. The length of vector c of our nanoribbon is 5.667 Å, which is larger than that of vector a (or b) (~ 3.182 Å) in the TMD monolayer in [2]. Our k grid is denser than that in [2]. So, we can estimate that our quasiparticle gap converged within 0.1 or less than 0.1 eV. For the optical calculation, Ref. 2 used a k-grid of $72 \times 72 \times 1$, equivalent to a distance of $0.0044/\text{Å}$ between two adjacent k points in vector a (or b) direction, see Table II in [2]. We used a k-grid of $1 \times 1 \times 36$ for our nanoribbon, and this is equivalent to a distance of $0.0049/\text{Å}$ between two adjacent k points in vector c (the ribbon length) direction. We checked the optical calculations with denser k-grids of $1 \times 1 \times 42$ and $1 \times 1 \times 48$, and found that the calculated optical spectra have almost no obvious difference from the three k-grids ($1 \times 1 \times 36$, $1 \times 1 \times 42$ and $1 \times 1 \times 48$), indicating the calculated optical properties are well converged results, see Figure S38 below.

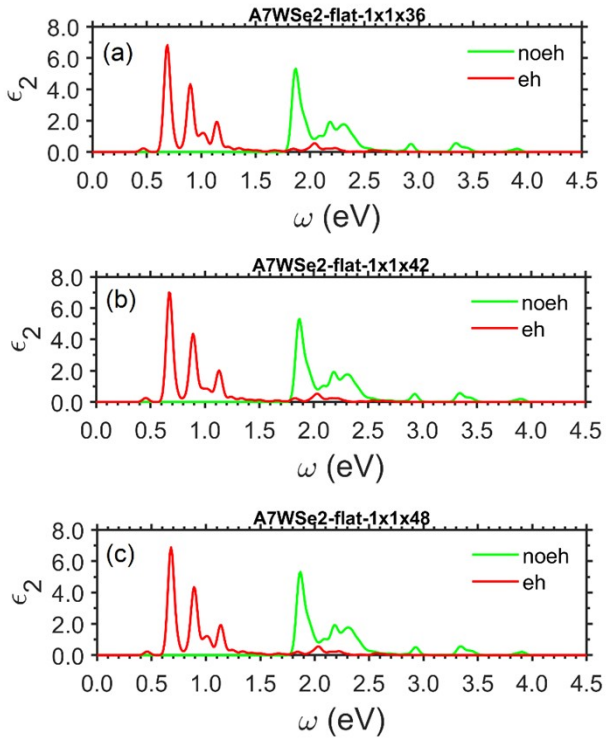

Figure S38. Comparison of the calculated optical absorption spectra of the flat A7WSe2 nanoribbon with three different fine k-grids (a) $1 \times 1 \times 36$, (b) $1 \times 1 \times 42$ and (c) $1 \times 1 \times 48$.

Reference

1. Manish Chhowalla, Hyeon Suk Shin, Goki Eda, Lain-Jong Li, Kian Ping Loh and Hua Zhang, The chemistry of two-dimensional layered transition metal dichalcogenide nanosheets, Nat. Chem., 2013, 5, 263.

2. Diana Y. Qiu, Felipe H. da Jornada, and Steven G. Louie, Optical Spectrum of MoS2: Many-Body Effects and Diversity of Exciton States, Phys. Rev. Lett. 111, 216805(2013).